A Holocene temperature (brGDGT) record from Garba Guracha, a high-altitude lake in Ethiopia.

Lucas Bittner[1], Cindy De Jonge[2], Graciela Gil-Romera[3,4], Henry F. Lamb[5,6], James M. Russell[7], Michael Zech[1]

[1)] Heisenberg Chair of Physical Geography with focus on paleoenvironmental research, Institute of Geography, Technische Universität Dresden, Dresden, Germany
[2)] Geological Institute, Department of Earth Sciences, ETH Swiss Federal Institute of Technology, 8092 Zurich, Switzerland
[3)] Plant Ecology and Geobotany dept., Philipps-Marburg University, Marburg, Germany.
[4)] Department of Geo-environmental Processes and Global Change, Pyrenean Institute of Ecology, CSIC, Zaragoza, Spain
[5)] Department of Geography and Earth Sciences, Aberystwyth University, Aberystwyth, UK.
[6)] Department of Botany, School of Natural Sciences, Trinity College Dublin, Dublin 2, Ireland
[7)] Department of Geological Sciences, Brown University, USA

Correspondence to: Lucas Bittner (lucas.bittner@tu-dresden.de)

Abstract. Eastern Africa has experienced strong climatic changes since the last deglaciation (15,000 years ago). The driving mechanisms and teleconnections of these spatially complex climate variations are yet not fully understood. Although previous studies on lake systems have ~~largely~~ enhanced our knowledge of Holocene precipitation variation in eastern Africa, relatively few ~~such~~ studies have reconstructed the terrestrial temperature history of eastern Africa from lake archives. Here, we present (i) a new branched glycerol dialkyl glycerol tetraether (brGDGT) temperature calibration that includes Bale Mountain surface sediments and (ii) a quantitative record of mean annual temperature (MAT) over the past 12 cal ka BP using brGDGTs in a sediment core collected from Garba Guracha (3950 m a.s.l.) in the Bale Mountains. After adding Bale Mountain surface sediment (n=11) data to the existing East African lake dataset, additional variation in 6-methyl brGDGTs was observed, which necessitated modifying the MBT'$_{5ME}$ calibration by adding 6-methyl brGDGT IIIa' (resulting in the MBT-Bale Mountain index, r^2=0.93, $p<0.05$). Comparing the MBT'$_{5ME}$ and the new MBT-Bale Mountain index, our high altitude Garba Guracha temperature record shows that ~~significant~~ warming occurred shortly after the Holocene onset~~.~~ when the temperature increased by more than 3.0 °C in less than 600 years. The highest temperatures prevailed between 9 and 6 cal ka BP, followed by a temperature decrease until 1.4 cal ka BP. The reconstructed temperature history is ~~strongly~~ linked to supraregional climatic changes associated with insolation forcing and the African Humid Period (AHP), as well as with local anomalies associated with catchment deglaciation and hydrology.

Keywords: paleolimnology; MAT; brGDGT, calibration, palaeoclimatology, eastern Africa

1. INTRODUCTION

The severity of the current climate change and its global implications have been widely discussed following the latest report from the Intergovernmental Panel for Climate Change (IPCC) (IPCC, 2021). Uncertainty in future climate projection highlights the need for the scientific community to use palaeoclimate to estimate climate baseline conditions prior to human impact on climate (Neukom et al., 2019). Although palaeoclimatology has become a central discipline in understanding current climate variability (Thompson et al., 2002), important areas of the planet remain understudied. A partial understanding of global climate complexity can lead to biased views of natural systems (Hughes et al., 2021). This is the case for the African continent in general and northeastern Africa in particular. Current climatic conditions in eastern Africa vary significantly due to its complex topography and the influence of the Intertropical Convergence

Zone (ITCZ), the Indian Monsoon and the El Niño-Southern Oscillation (ENSO). All of these affect temperature and the distribution, amount and timing of rainfall in the region, resulting in a wide range of climatic conditions from the warm, dry and semi-arid conditions of northern Kenya, south-eastern Ethiopia, Djibouti and Somalia to the cool, humid conditions of the western highlands (Hove et al., 2011; Nicholson, 2017; Lyon and Vigaud, 2017).

There is clear evidence indicating that, since the last glacial period, northern and eastern Africa experienced severe climatic changes (Tierney et al., 2008, 2011a, 2017, 2013; Loomis et al., 2015; Wagner et al., 2018). Three major climate events are the post-glacial warming (~15 ka BP), ~~the~~ hydrological variability during the African Humid Period (AHP) (15 -5 ka BP) (deMenocal et al., 2000)~~,~~ that lead to the greening of the Saharan Desert (Blom et al., 2009), and the drying period near the beginning of the Meghalayan (4.2 ka BP) (Bini et al., 2019). The intensity and the timing of these climatic changes varied regionally over northern and eastern Africa (Castañeda et al., 2016). While the driving mechanisms and the regional differences are complex and not fully understood, evidence supports the view that climatic changes in northern and eastern Africa were connected across the northern hemisphere (Tierney et al., 2013; Tierney and Russell, 2007; Otto-Bliesner et al., 2014). These complex teleconnections and their global impact support the importance of understanding long-term climate drivers in eastern Africa. Such knowledge will lead to better assessments of the impacts and potential mitigation of the current and future climate change scenarios in this world's understudied yet critical region.

While several studies have reconstructed the precipitation history in ~~Northern~~ northern and eastern Africa over the last 15 cal ka BP (Bittner et al., 2021; Costa et al., 2014; Jaeschke et al., 2020; Junginger et al., 2014; Morrissey and Scholz, 2014; Tierney et al., 2011a; Trauth et al., 2018; Wagner et al., 2018), only a few have reconstructed the regional temperature history in northern and eastern Africa (Castañeda et al., 2016; Morrissey et al., 2018; Berke et al., 2012a; Loomis et al., 2017, 2012, 2015; Tierney et al., 2008, 2016). Moreover, there is a lack of terrestrial temperature reconstructions, especially in the high altitudes and the Horn of Africa. The Bale Mountain, situated in the East of the Rift Valley, are a valuable study site with the potential to enhance the paleoclimatic knowledge in an understudied region.

For terrestrial archives, different methods have been developed and applied based on pollen, chironomids, and lipid biomarkers (Cheddadi et al., 1998; Wu et al., 2007; Chevalier and Chase, 2015; Bonnefille et al., 1992; Eggermont et al., 2010; Schouten et al., 2007). Over the last 15 years, an innovative approach for temperature reconstructions

emerged based on branched glycerol dialkyl glycerol tetraethers (brGDGTs), membrane-spanning bacterial lipids (Damsté et al., 2000). Several calibration studies in different settings (i.e. soils and lakes) have shown a correlation between brGDGT abundances and mean annual air temperature (MAT) (e.g. De Jonge et al., 2014; Dearing Crampton-Flood et al., 2020; Russell et al., 2018; Weijers et al., 2007). These calibrations have been successfully used to quantitatively reconstruct continental temperature in marine river outflow and lacustrine sediments and terrestrial archives such as loess sequences and paleosoils (Loomis et al., 2015, 2017; Schreuder et al., 2016; Zeng and Yang, 2019; Garelick et al., 2022). Recently, global calibrations have been developed that suit cooler and more seasonal high-latitude lakes better (Martínez-Sosa et al., 2021; Raberg et al., 2021).

The phylogenetic breadth of the brGDGT-producing bacteria is still poorly constrained, although members from the phylum Acidobacteria have been proposed to produce brGDGTs both in cultures and in the environment (Sinninghe Damsté et al., 2018; De Jonge et al., 2019, 2021; Weber et al., 2018; van Bree et al., 2020). A recent study by Halamka et al., 2021 reports that Acidobacteria produce certain brGDGTs under oxygen limitation. Originally, Weijers et al. (2007b) found that the methylation (MBT) and ~~cyclization~~ cyclisation of branched tetraethers (CBT) correlate with the measured mean annual air temperature (MAT) and pH values, respectively. Following the analytical separation of 5 and 6 methyl isomers, De Jonge et al. (2014) developed a new modified MBT'_{5ME} ratio. This resulted in a revised calibration that removed the pH dependence affecting the MBT/MAT correlation and improved the accuracy of MAT reconstructions in terrestrial/soil archives. As brGDGT distributions recovered from lake sediments showed a different MAT dependence compared to soils, Russell et al. (2018) developed a MBT'_{5ME} temperature calibration for lake sediments in eastern Africa. However, compared to the dataset of Russell et al. (2018), the brGDGT distribution of some Bale Mountain lake surface sediments are unique (Baxter et al., 2019). Although the MBT'_{5ME} calibration by Russell et al. (2018) is a valuable supra-regional metric for reconstructing lake temperature, an adjusted calibration might better account for local conditions in the Bale region.

In this study, we aim to (i) compare brGDGT distributions from lake surface sediments of the Bale Mountains (n=11) (Baxter et al., 2019) with the eastern African dataset (Russell et al., 2018), (ii) develop a new ratio that captures the unique variation in the Bale Mountains and compare the accuracy of this calibrated ratio with the MBT'_{5ME}, and (iii) reconstruct the first Horn of Africa high altitude paleotemperature record in the Bale Mountains using the sedimentary record of Garba Guracha (3950 m a.s.l.) and (iv) compare this Garba Guracha temperature record with other records in the region.

2. REGIONAL SETTINGS

2.1 Study area

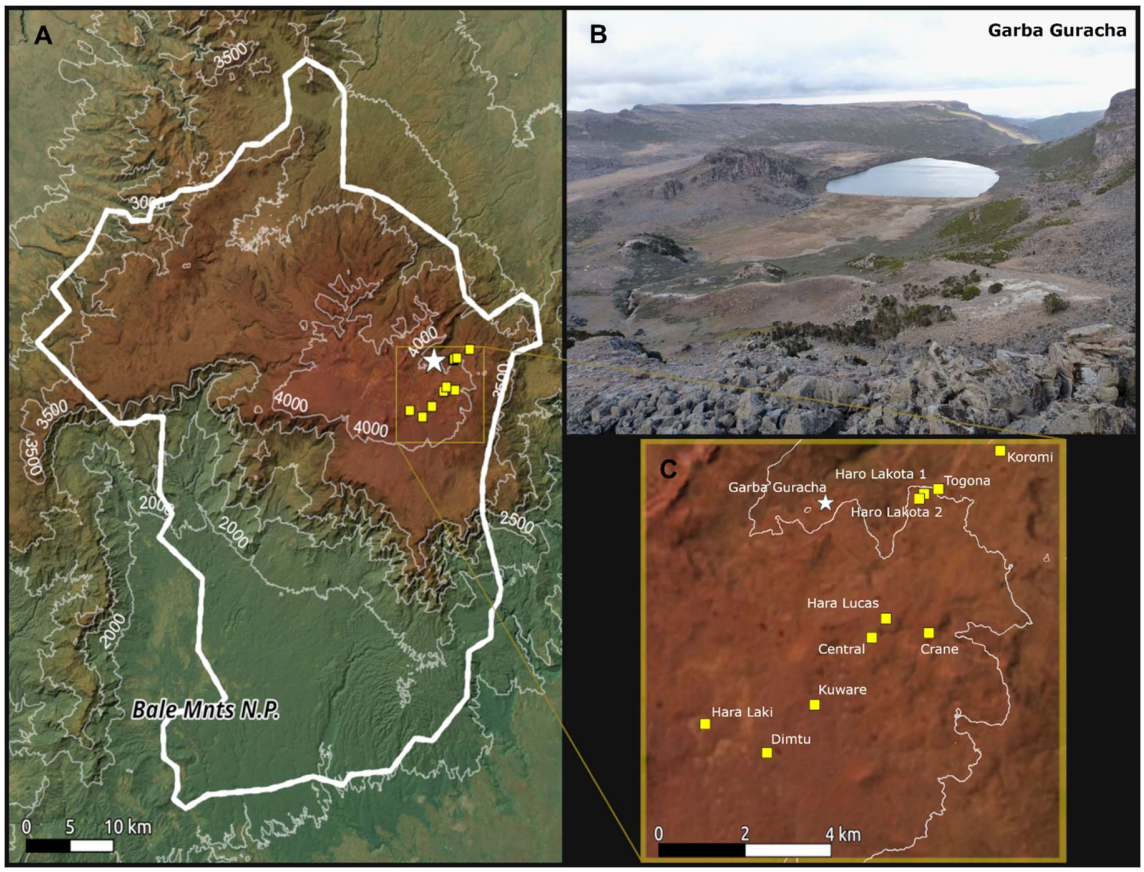

Figure 1: Location of the study area. (A) Bale Mountain National Park (thick white line), (B) a northeastward view over the glacial cirque of the Garba Guracha catchment (Bittner et al., 2021), and (C) Bale Mountain lakes in the dataset (yellow) - The map was created by the authors using QGis 3.24 Tisler. All map layers are CC-by-SA v4.0, Image is from Bing Image / DigitalGlobe © Microsoft, DEM is from NASA/JPL SRTM (http://www.jpl.nasa.gov/srtm/) and the Bale Mountains National Park boundaries are from © OpenStreetMap contributors 2019. Distributed under the Open Data Commons Open Database License (ODbL) v1.0.

Garba Guracha (6.875781N, 39.878075E; Fig. 1) and all other lakes in this study are located east of the Main Ethiopian Rift in the Bale Mountains of the Bale-Arsi Massif. More specifically, they are situated on the Sanetti Plateau, the highest plateau in the Bale Mountains, between ~3800 to ~4200 m.a.s.l. and an area of 600 km^2 (Osmaston et al., 2005). Solidified horizontal lava consisting of tuffs with rhyolites, alkali basalt, and trachyte formed the volcanic plateau (Uhlig and Uhlig, 1991; Williams, 2016). The plateau and the valleys were partially glaciated at the Last Glacial Maximum (Groos et al., 2021, 2020; Osmaston et al., 2005; Ossendorf et al., 2019). The glacial cirque Garba

Guracha was first mentioned by Werdecker (1962) and was also described in depth by Umer et al. (2007) and Tiercelin et al. (2008). With a maximum water depth of 6 m and a very small catchment area, the lake is located at 3950 m above sea level. (0.15 km^2; Fig. 1). The bedrock of the catchment is carbonate-poor (Löffler, 1978; Uhlig and Uhlig, 1991). An outlet towards the Togona Valley is present during the rainy season at the lake's northern end. A swampy alluvial plain fed by multiple springs stretches along the lake's southern shore.

2.2 Climate

The climate of the Bale Mountains varies spatially and temporally, affected by the orographic differences in altitude, a north-south exposure and by changing atmospheric air mass movements over the course of the year (Kidane et al., 2012; Uhlig and Uhlig, 1991). The Bale Mountains experience a four-month dry season (November to February) and a long wet season with complex orographic rainfall patterns (March to October) (Woldu et al., 1989; Kidane et al., 2012). The complexity of the rainfall pattern is associated with the convergence of northeast and southwest winds due to the northern and southern location of the ITCZ between June and September and between October and March, respectively (Tiercelin et al., 2008; Kidane et al., 2012). The Equatorial Westerlies and the Indian Ocean monsoon act as two moisture sources for the precipitation in the Bale Mountains (Miehe and Miehe, 1994; Uhlig, 1988). With 1000-1500 mm per year, the southern part of Bale Mountain experiences the highest precipitation amount, whereas the northern region, including Garba Guracha, only receives 800-1000 mm (Woldu et al., 1989). Temperatures vary seasonally, with the lowest temperatures in the dry season and the highest temperatures in the rainy season (Hillman, 1988). The Afro-Alpine regions, including the Sanetti Plateau, are ~~characterized~~ characterised by diurnal temperature differences between day and night (-15 to +26°C) (Hillman, 1988). Across the Bale Mountains, climate data has been collected since 2017 with a mean annual temperature of 4.9 °C (max. 6°C; min. 3.4 °C) at the Angesso Station, located at the same altitude 4 km northeast of Garba Guracha. The mean annual temperature at Garba Guracha is 5.4°C (Baxter et al., 2019).

3. MATERIAL AND METHODS

3.1. Material and Sampling

In this study, we used the published data of 76 surface sediment samples from eastern African lakes. ~~These lake sediments~~The data of these lakes, located mainly in Ethiopia, Uganda and Kenya, ~~were analyzed, and the results~~ were published by Loomis et al. (2014, 2011, 2012), Russell et al. (2018), Eggermont et al. (2011) and Baxter et al. (2019). The environmental data for the 11 lakes in the Bale Mountains were published by Eggermont et al. (2011) and Baxter et al. (2019), and the corresponding MAT is based on a calculated lapse rate supported by local climate station data (Loomis et al., 2012; Russell et al., 2018).

At the Garba Guracha site, two overlapping sediment cores were retrieved in February 2017, at a water depth of 4.8 m using a Livingstone piston corer. A maximum sediment depth of 1550 cm was reached, covering an organic matter-rich upper section (0-900 cm) and an organic matter-poor bottom one (900-1550 cm). This study focuses on the last 12.3 cal ka BP covering the 0-950 cm, with a mean sedimentation rate of 15 years/cm (more details on sediment properties and chronology can be found in Bittner et al. (2020)). We sampled at contiguous 10 cm intervals (average ~100 years of sedimentation). Thirty-five samples were selected for brGDGT analyses.

3.2 Sample preparation and analysis

The total lipid extracts (TLE) of the surface sediment samples were extracted using an accelerated solvent extractor (ASE) with dichloromethane:methanol in a ratio of 9:1 (Loomis et al., 2012). The brGDGTs were purified and separated according to their polarity. The samples were quantified following the method described by Huguet et al. (2006).

The TLE of the downcore sediments was obtained using a soxhlet system by constant rinsing (24h) with solvent (dichloromethane:methanol in a ratio of 9:1). After rotary evaporation, the TLE was redissolved in *n*-hexane and transferred onto a pipette column filled with aminopropyl silica gel (Supelco, 45 um). Solvents of increasing polarity (*n*-hexane, dichloromethane/methanol 2:1; diethyl ether/acetic acid 19:1) were used to selectively elute the fractions of the TLE (nonpolar fraction A; two polar fractions B and C, including brGDGTs). Fraction B contained 98-99%, while fraction C contained 1-2% of all brGDGTs. All results refer to the brGDGTs contained in fraction B. Before measurement, a C_{46} brGDGT standard was added, and the extract dried, redissolved in n-hexane/isopropanol (99:1) and filtered using a 0.45 um polytetrafluoroethylene (PTFE) filter. The measurements of the GDGTs (dissolved in n-

hexane/IPA (99:1)) were done at ETH Zurich using a high-performance liquid chromatograph (Agilent 1260) coupled to a quadrupole mass spectrometer configured for atmospheric pressure chemical ~~ionization~~ ionisation (HPLC-APCI-MS). The separation of the GDGTs was achieved by two silica columns at 45°C (modified after Hopmans et al. (2016)) with a flow rate of 0.2ml/min and an injection volume of 10 µl. Compound-peak integrations of *m/z* 1292, 1050, 1048, 1046, 1046, 1034, 1032, 1022, 1020, 1018 and 744 were performed according to previously published methods (Hopmans et al., 2016).

3.3 BrGDGTs – structure, statistical methods and proxy calculation

BrGDGTs can be present as tetra- (I), penta- (II), or hexamethylated (III) compounds with different numbers of cyclopentyl moieties (none (a), one (b), or two (c)). The outer methyl group can be positioned on the α and/or ω C5 (5-methyl compounds) or C6 (6-methyl compounds, indicated by a prime notation) location (De Jonge et al., 2014). To interpret the GDGT composition of the samples, we used the BIT, MBT', MBT'_{5ME}, and CBT' (Table 1).

We calculated the BIT index following the equation of Hopmans et al. (2004):

$$BITindex = (Ia + IIa + IIIa + IIa' + IIIa')/(Ia + IIa + IIIa + IIa' + IIIa' + crenarchaeol) \quad \text{[Eq. 1]}$$

De Jonge et al. (2014) showed that the MBT' ratio (Peterse et al., 2012) contains 5- and 6-methyl compounds that are explicitly mentioned here:

$$MBT' = (Ia + Ib + Ic)/(Ia + Ib + Ic + IIa + IIa' + IIb + IIb' + IIc + IIc' + IIIa + IIIa') \quad \text{[Eq. 2]}$$

By removing the 6 methyl isomers from the equation, De Jonge et al. (2014) improved the temperature calibration further:

$$MBT'_{5ME} = (Ia + Ib + Ic)/(Ia + Ib + Ic + IIa + IIb + IIc + IIIa) \quad \text{[Eq. 3]}$$

The ~~cyclization~~ cyclisation of branched tetraethers (CBT') is calculated following the equation from De Jonge et al. (2014a):

$$CBT' = {}^{10}log\,(Ic + IIa' + IIb' + IIc' + IIIa' + IIIb' + IIIc')/(Ia + IIa + IIIa) \quad \text{[Eq. 4]}$$

Russell et al. (2018) defined a calculation for surface water pH:

$$Surface\ water\ pH = 8.95 + 2.65 * CBT' \quad \text{[Eq. 5]}$$

Lake water conductivity can be calculated using the Eq. 12 of (Raberg et al., 2021):

$$ln(conductivity) = 6.62 + 8.87 * (Ib/(Ia + Ib + Ic))$$

$$+ 5.12 * ((IIa'/(IIa + IIb + IIc + IIa' + IIb' + IIc'))^2)$$

$$+ 10.64 * ((IIa/(IIa + IIb + IIc + IIa' + IIb' + IIc'))^2)$$

$$- 8.59 * (IIa/(IIa + IIb + IIc + IIa' + IIb' + IIc'))$$

$$- 4.32 * ((IIIa'/(IIIa + IIIb + IIIc + IIIa' + IIIb' + IIIc'))^2)$$

$$- 5.31 * ((IIIa/(IIIa + IIIb + IIIc + IIIa' + IIIb' + IIIc'))^2)$$

$$- 142.67 * ((IIIb/(IIIa + IIIb + IIIc + IIIa' + IIIb' + IIIc'))^2) \quad \text{[Eq. 6]}$$

The fractional abundance of any individual brGDGT compound (i) was defined as:

$$f(i) = i/(Ia + Ib + Ic + IIa + IIa' + IIb + IIb' + IIc + IIc' + IIIa + IIIa' + IIIb + IIIb' + IIIc + IIIc') \quad \text{[Eq. 67]}$$

3.4 Quantitative data analyses

Numerical analyses in this paper have been performed with Excel and R 4.1.0 (R Core Team, 2021). Results are displayed using the arithmetic mean and standard deviations using the notation ±. To explore the correlations ~~level~~ between brGDGTs and MAT, we used linear regressions and the reported Pearson correlation values (r^2), where ~~significant~~ correlations were considered significant when the p-value < 0.05. We performed a Principal Component Analysis (PCA) of brGDGTs from i) the calibration dataset and ii) the Garba Guracha record, based on ~~standardized~~ standardised and scaled fractional abundance. The ordination methods provide a simple yet effective way to ~~visualize~~ visualise the variability within the distribution of the brGDGTs. PCA was performed with the R package *factoextra* (Kassambara and Mundt, 2020).

4. RESULTS

4.1 BrGDGT patterns of surface sediments from lakes in the Bale Mountains

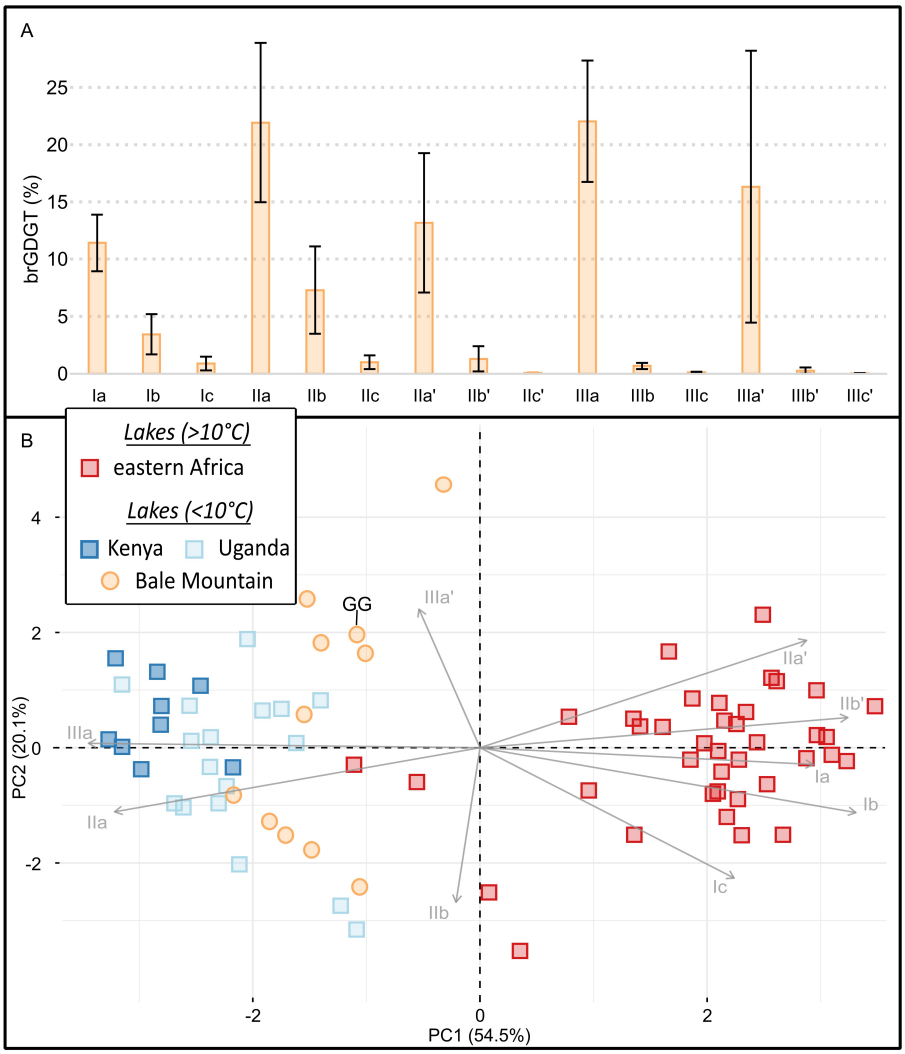

Figure 2: (A) Barplot of average brGDGT percentages in Bale Mountain lake surface sediments (Baxter et al., 2019), with standard deviation plotted as error flags and (B) PCA of brGDGTs of eastern African lakes with regional pattern; data from Russell et al. (2018) and Baxter et al. (2019) - lakes >10°C (~~purple~~red) and lakes <10°C (~~red~~Bale Mountain - orange, ~~turquoise~~ Kenya - blue and ~~green~~Uganda - light blue); Garba Guracha (GG).

To frame the downcore variation in Garba Guracha in the current environmental settings, we have expanded the dataset of Russell et al. (2018) by 11 Bale Mountain lake surface sediment samples (Table S1 and S2) (data from Baxter et al., 2019). Due to the missing values of IIc, IIc', IIIb, IIIb', IIIc and IIIc' in the manuscript by Russell et al. (2018), we

excluded these isomers in the Bale Mountain data from the PCA to allow direct comparison of the PCAs (see the supplementary Figure S1 for~~for a~~ different PCA including all isomers). The highest fractional abundances of brGDGTs in these surface sediments are (i) IIIa with a mean of 22% (±5), (ii) IIa with a mean of 22% (±7) and (iii) IIIa' with a mean of 16% (±12) (Fig. 2A, Table S2).

The PCA of brGDGTs shows some differences between the East African lake dataset and the Bale Mountain lakes (Fig. 2B). IIIa and IIa have negative loadings, and IIa', IIb', Ia, Ib and Ic have positive loading on PC1. PC2 ~~has~~ shows negative loadings from IIb and positive loading from IIIa' and IIa'. The Bale Mountain lakes have a negative score on PC1, consistent with their location in a cool climate. The similar distribution of tetra-, penta- and hexamethylated brGDGTs in surface sediments, illustrates a shared dominant lake-derived provenance as the East African lake dataset, as soil-derived brGDGTs are characterized by a larger fractional abundance of brGDGTs Ia (Russell et al., 2018). At the same time, the Bale Mountain lakes have a wide~~r~~ dispersion on PC2, illustrating additional variation of brGDGTs. Regional differences in the brGDGT isomer abundances, especially in Bale Mountain surface sediments, are further supported by variations in the degree of cyclisation (DC') and CBT' ratio values in the eastern African lake surface sediment data (Russell et al., 2018; Baxter et al., 2019) (Fig. S~~3~~2). Specifically, ~~On~~on PC2, a decrease ~~of 5$_{ME}$ cyclopentane of brGDGTs~~ IIb and an increase of ~~6 ME brGDGT~~ IIIa' is visible in some of the Bale Mountain lakes, including Garba Guracha (highlighted in Fig. 2B).

Compared to similar ~~high~~ high-altitude lakes (above 3500 m and MAT < 10°C) in eastern Africa (~~situated in~~ Kenya and Uganda lakes previously published in the East African lake dataset (Russell et al., 2018)), the percentage of IIIa and IIa is lower, and the percentage of IIIa' and IIa' is higher in the Bale Mountain lakes (Fig 3). Interestingly, the combined percentage of these 5 and 6 methyl isomers is similar (Fig. 3-A).

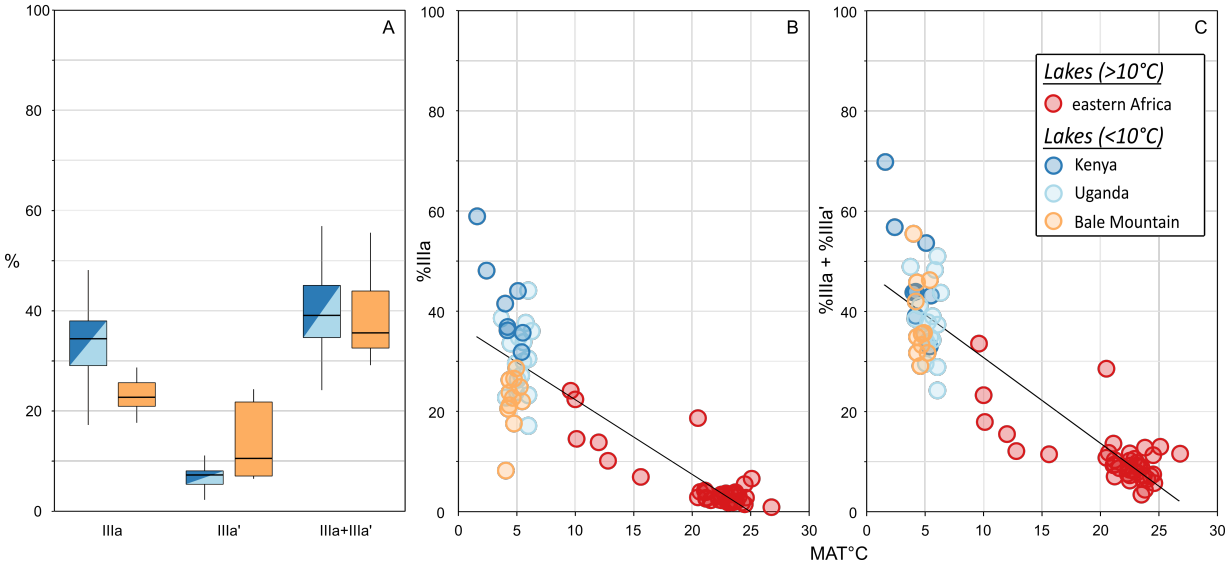

Figure 3: (A) Abundance (%) of IIIa and IIIa'; (B) Linear correlation between IIIa (%) and MAT (r^2 = 0.78) and (C) IIIa + IIIa' (%) to MAT (r^2 = 0.82) - data from Russell et al. (2018) and Baxter et al. (2019) - lakes >10°C (red) and lakes <10°C (Bale Mountain - orange, Kenya - blue and Uganda - light blue)~~data from Russell et al. (2018) - lakes >10°C (purple) and lakes <10°C (red and green); Bale Mountain lakes (Baxter et al., 2019) (turquoise)~~.

We ~~hypothesize~~ hypothesise that the 6-methyl compound (IIa' and IIIa') ~~is~~ might be produced instead of their 5-methyl counterparts (IIa and IIIa), ~~or~~resulting in their ~~in~~ higher fractional abundances~~,~~ in some of the Bale Mountain lakes (Fig. 3A). This is supported by our observation that~~Moreover~~, in the East African lake dataset, the correlation of %IIIa to MAT (r^2 = 0.78) is slightly improved by adding %IIIa' to r^2 = 0.82 (Fig 3 B~~, and~~ C). Narrowing the temperature range, ~~In eastern African lakes with temperatures lower 10°C~~(MAT<10 °C), the improvement remains significant: the correlation of %IIIa to MAT (r^2 = 0.11; p-value < 0.001) is improved by adding %IIIa' to r^2 = 0.31 (p-value < 0.001) (Fig. S3). Although the production of IIIa' at the expense of IIIa is poorly understood in lacustrine settings the isomerisation of brGDGTs can be affected by the conductivity and salinity of the lake water (Raberg et al., 2021; Wang et al., 2021). As IIIa is a major component of the MBT'$_{5ME}$ ratio, the hypothesised production of IIIa' at the expense of IIIa could have the potential to influence MBT'$_{5ME}$ values.~~Although the production of IIIa' at the expense of IIIa is poorly understood in lacustrine settings, it clearly has the potential to influence MBT'$_{5ME}$ values.~~ Indeed, MBT'$_{5ME}$ values of the Bale Mountain lakes range from 0.20 to 0.37, with a mean of 0.24 (±0.05). As the MAT range of Bale Mountain lakes is limited (4-5.4 °C), the range of MBT'$_{5ME}$ is larger than expected of the measured MAT relative to similar eastern African lakes in the East African lake dataset (MBT'$_{5ME}$ = 0.17 to 0.25 with a mean of 0.22 ± 0.02; MAT = 4-5.4 °C) (Russell et al., 2018). ~~Regional differences in the brGDGT isomer abundances, especially in Bale~~

~~Mountain surface sediments, are further supported by variations in the degree of cyclisation (DC') and CBT' in the eastern African lake surface sediment data (Russell et al., 2018; Baxter et al., 2019) (Fig. S3).Moreover, regional variations in brGDGT isomers, especially in Bale Mountain surface sediments, appear in the degree of cyclization (DC') and CBT' in the eastern African lake surface sediment data (Fig. S2).~~

4.2 BrGDGT patterns of the Garba Guracha sediment core

In general, the sediments of the Garba Guracha are characterised by a high input of aquatic organic matter. Several analysed proxies used to identify the source of organic matter indicate a predominantly aquatic production ($\delta^{13}C$, TOC/N, P_{aq}, sugar quantification ratios) (Bittner et al., 2020, 2021). The composition of brGDGTs in the sediment of Lake Garba Gurahca is inconsistent with the soil samples in Bale Mountain, indicating different producing communities (Fig. S4, Table S3). These findings are concurrent with the results of Russell et al. (2018) that brGDGTs in eastern African lake sediments are dominantly lake-derived. Therefore, we suggest that most brGDGTs in the Garba Guracha sediment archive are also of aquatic origin.

In the Garba Guracha sediments, both branched and isoprenoid GDGTs are present. The BIT index ranges between 0.8 and 1 (mean=0.98, ± 0.04). Only the oldest samples (12-10 cal ka BP) have a lower BIT index value of 0.8 to 0.9 (Table ~~S3~~S4). Tetramethylated brGDGTs in the sediment core represent on average 19.5%, pentamethylated brGDGTs 44%, and hexamethylated brGDGTs 36.5% (Table ~~S3~~S4). The highest fractional abundances are (i) IIIa with a mean of 21% (±5), (ii) IIa with a mean of 20% (±3) and (iii) Ia with a mean of 15% (±3). The MBT'_{5ME} ranges from 0.20 to 0.35 with a mean of 0.28 (±0.04) (Table ~~S4~~S5). The CBT' ratio ranges from 0.06 to -0.54 with a mean of 0.27 (±0.18) (Table ~~S3~~S4).

A PCA of all downcore brGDGTs distributions (Fig. 4A) shows that the first two components explain 63.2% of the variance. On PC1 (42.3%), all 6 methyl isomers have negative loadings, while 5 methyl isomers show positive loadings. PC2 (20.9%) shows positive loadings of all hexamethylated brGDGTs and negative loadings of all penta- and tetramethylated brGDGTs. The PCA reveals changes in brGDGT composition with core depth when the data points are grouped using the following age cut-offs: (0-4.3 cal ka BP; 4.3-10.5 cal ka BP; 10.5-12.5 cal ka BP) (Fig. 4A). In phase 1 (12.5 – 10.5 cal ka BP), IIIa, IIIa' and IIa have the highest mean abundances of 30%, 17%, and 17%, respectively. In phase 2 (10.5 – 4.3 cal ka BP), the mean abundance of IIIa and IIIa' are decreased by around 9%, while IIa, IIb and Ia increase. In phase 3 (4.3 – 0 cal ka BP), the mean abundances of IIIa decrease by 6% further. Conversely,

298 the mean abundance of IIIa' increases again by 12%. The same holds true for IIa (-5%) and IIa' (+6%). The mean
299 abundance of Ia increases further by 3% (Fig 4B).
300

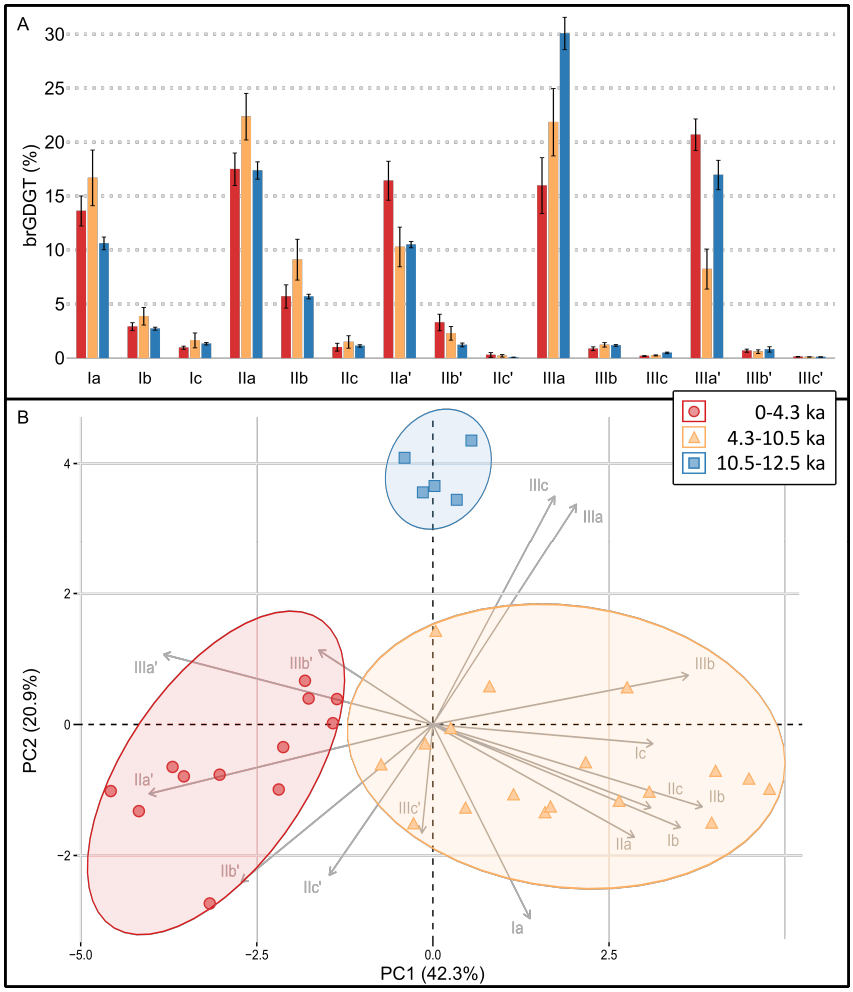

301

302 Figure 4: (A) barplot of average brGDGT percentages in the Garba Guracha sediment core, with standard deviation plotted as error flags; (B) PCA
303 of brGDGTs of the Garba Guracha sediment core; data from 0 to 4.3 cal ka BP (red), data from 4.3 to 10.5 cal ka BP (orange) and data from 10.5
304 to 12.5 cal ka BP (blue).~~; (B) barplot of average brGDGT percentages in the Garba Guracha sediment core, with standard deviation plotted as error~~
305 ~~flags.~~

306

307 The unusually high abundance of brGDGTs IIIa' compared to IIIa observed in surface sediments of Bale Mountains
308 lakes (Fig. 2A) is also visible in the Garba Guracha record and the relative abundance of IIIa' varies with depth. High
309 amounts of IIIa' appear until 10.8 cal ka BP followed by low percentage (<10%) until 4.5 cal ka BP. The highest
310 abundance of IIIa' with up to 22% occurs after 4.5 cal ka BP until the recent past. The changing abundances of IIIa' in
311 our record coincide with changes in CBT' (Fig. 5). The variability in the 6-methyl brGDGTs reflects the largest part

of the variation in this dataset, reflected by the good agreement (r^2= 0.77, p<0.001) between the fractional abundance of brGDGTs IIIa' and the sample loadings on PC1.

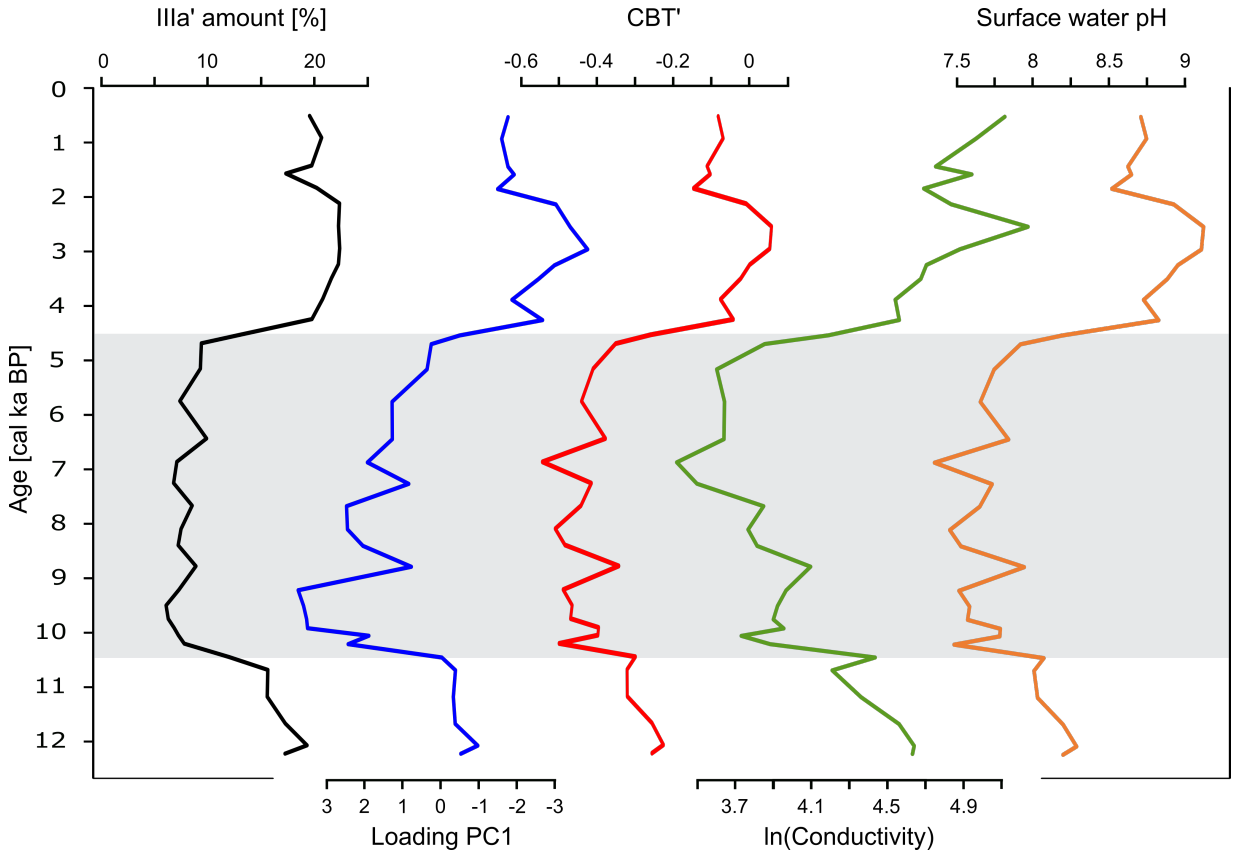

Figure 5: Downcore functions for IIIa' amount, the PC1 loading, CBT', ln(conductivity) (Eq. 12 in Raberg et al., 2021), and surface water pH of the Garba Guracha brGDGT record.

5. DISCUSSION

5.1 Possible MAT calibration functions inferred from the expanded eastern African surface sediment dataset

Table 1: Temperature calibrations – Ratios, calibration dataset, r^2, and root-mean-square-error (RMSE) in °C - East African Lake dataset (EAL), East African Lakes + Bale Mountain lakes (EAL_{BM})

Ratio	Calibration dataset	r^2	RMSE °C
MBT'_{5ME} (Ia+Ib+Ic)/(Ia+Ib+Ic+IIa+IIb+IIc+IIIa)	EAL (n=65)	0.92	2.41
	EAL_{BM} (n=76)	0.92	2.41
MBT'_{5ME} + IIIa' (Ia+Ib+Ic)/(Ia+Ib+Ic+IIa+IIb+IIc+IIIa+IIIa') [Eq. 6~~8~~]	EAL_{BM} (n=76)	0.93	2.38
Simplified MBT'_{5ME} + IIa'&IIIa' Ia/(Ia+IIa+IIIa+IIa'+IIIa') [Eq. ~~7~~9]	EAL_{BM} (n=76)	0.84	3.48
Simplified MBT'_{5ME} + IIIa' Ia/(Ia+IIa+IIIa+IIIa') – [Eq. ~~8~~10]	EAL_{BM} (n=76)	0.91	2.59

We added the GDGT distribution data of 11 surface sediments from Bale Mountain~~s~~ lakes (Baxter et al., 2019) to the existing data of Russell et al. (2018) and applied the MBT'_{5ME} calibration (Table 1). Here, the original dataset (n = 65) is referred to as East African Lakes "EAL", while the extended dataset (n = 76) is referred to as East African Lakes + Bale Mountain lakes (EAL_{BM}). The linear correlation between the MBT'_{5ME} and MAT was almost identical after adding the 11 Bale Mountain lake samples (EAL r^2= 0.92, EAL_{BM} r^2 = 0.~~93~~92). In the tropical Bale Mountain, ~~especially due to the intense insolation~~, the freezing of lakes is extremely rare, due in part to the intense year-round insolation, and MAT is equal to MAF. To test whether the unique brGDGT distribution in some Bale Mountain lakes (Fig. 2) affected the temperature correlation, we applied various calibrations to account for the increased abundance of IIIa' (and to a lesser extent IIa'). ~~Including these compounds is *a priori* supported by global scale calibrations, as Raberg et al. (2021) showed that a global temperature calibration with a modified MBT' ratio that includes IIIa' and IIa' (Table 6, Eq. 7) correlates with month above freezing (MAF) in lakes (r^2 = 0.90, RMSE= 2.18) almost as well as the unmodified MBT'_{5ME} ratio.~~ In the EAL_{BM} dataset, the application of this ratio has a lower r^2 of 0.84 and a higher RMSE of 3.48°C compared to the MBT'_{5ME} (Table 1: Eq. ~~7~~9). As brGDGT IIIa' specifically was shown to increase in Bale Mountain sediments and improved the correlation with MAT (Fig. 3B and C), we investigated alternative ratios that incorporate this compound but exclude IIa'. Table 1 and Fig. 6 ~~summarize~~ summarise the correlation coefficients of the MBT'_{5ME}

(r^2 = 0.92, RMSE of 2.41°C), an MBT'_{5ME} ratio that includes IIIa' (Eq. ~~6~~10) with r^2 = 0.93 and RMSE of 2.38°C and the simplified ratio that includes only the major brGDGTs compounds (Eq. ~~8~~10: r^2 = 0.91 and an RMSE of 2.59°C).

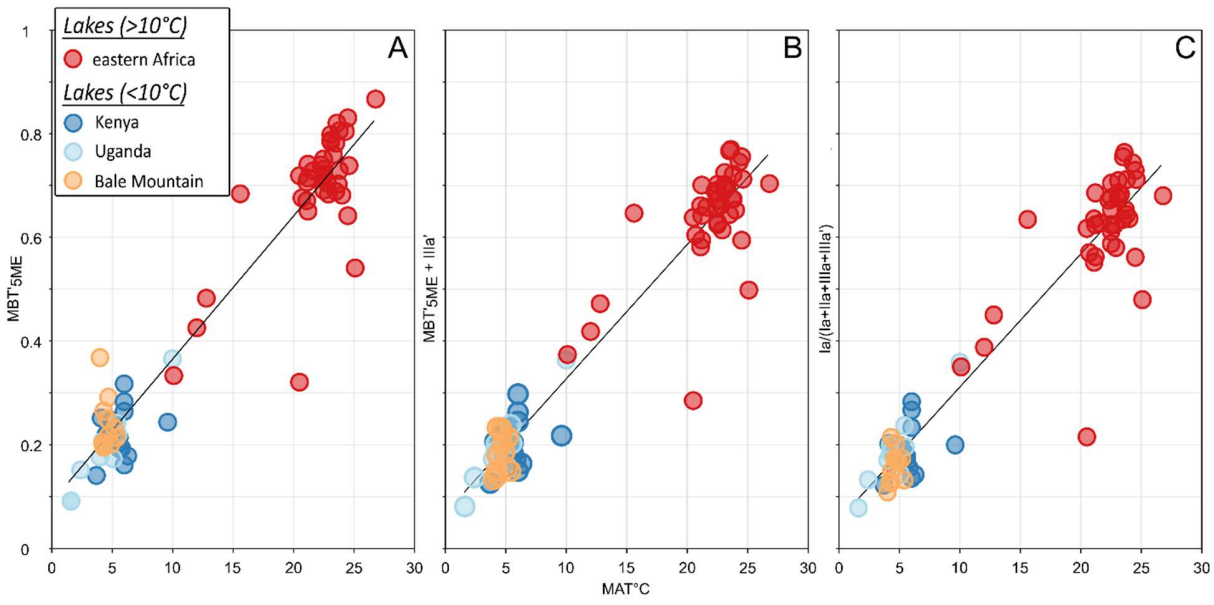

Figure 6: Correlations EAL_{BM} datasets, (A) MBT'_{5ME} (r^2 = 0.92; RMSE of 2.41); (B) MBT'_{5ME} + IIIa' (r^2 = 0.93; RMSE of 2.38).); (C) Ia/(Ia+IIa+IIIa+IIIa') (r^2 = 0.91; RMSE of 2.59) - data from Russell et al. (2018) and Baxter et al. (2019) - lakes >10°C (red) and lakes <10°C (Bale Mountain - yellow, Kenya - blue and Uganda - light blue)~~data from Russell et al. (2018) - lakes >10°C (purple) and lakes <10°C (red and green); Bale Mountain lakes (Baxter et al., 2019) (turquoise).~~

The results of the calibrations Ia/(Ia+IIa+IIIa+IIIa') (MAT= -0.773 + 35.646 x Ia/(Ia+IIa+IIIa+IIIa')) and MBT'_{5ME} + IIIa' (MAT= -1.4734 + 35.777 x MBT'_{5ME} + IIIa') ~~calibrations~~ applied to the Garba Guracha sediment core are very similar and correlate well (r^2=0.97) (Fig. 7, purple and green curves, respectively). Therefore, we will only discuss ~~only~~ the best performing calibrations developed using the EAL_{BM} dataset ~~performing~~ MBT'_{5ME} (MAT= -1.8299 + 33.304 x MBT'_{5ME}) and the MBT'_{5ME} + IIIa' calibration ~~developed using the EAL_{BM} dataset~~ to the downcore distributions.

5.2 Paleotemperature reconstructions for the Garba Guracha sedimentary record - comparison of the different calibrations

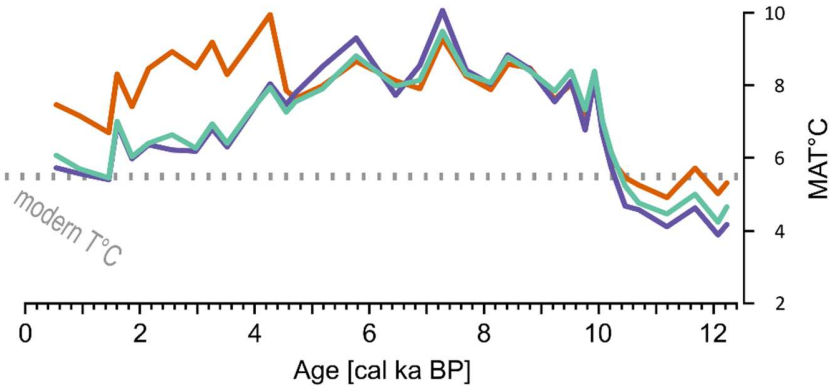

Figure 7: Reconstructed temperatures of the Garba Guracha sedimentary record. MBT'$_{5ME}$ (orange); Ia/(Ia+IIa+IIIa+IIIa') (purple); MBT'$_{5ME}$ + IIIa' (turquoise).

We evaluate the downcore trend in GG sediments to compare the performance of both calibrations, revealing periods of agreement (10-4.2 ka BP) and a period of temperature offset (since 4.2 ka BP). Using established and newly developed ratios and calibrations (~~Russell et al., 2018; this paper~~MBT'$_{5ME}$ +IIIa' and MBT'$_{5ME}$ EAL$_{BM}$) resulted in similar absolute values and comparable temperature trends, principally in the early and mid-Holocene. Reconstructed temperatures range from 4.9 to 10.0°C (MBT'$_{5ME}$) and 4.2 to 9.5°C (MBT'$_{5ME}$ + IIIa') (Fig. 7). Despite a slightly different range in temperature (4.4 and 5.3 °C), the trends of both calibrations are similar between 12 and 4.7 cal ka BP. The lowest MATs (< 5°C) occurred between 12.2 cal ka BP (950 cm) and 10.5 cal ka BP (800 cm). MAT increased rapidly by 3.5°C between 10.5 cal ka BP (800 cm) and ca. 10 cal ka BP (700 cm). During the early to mid-Holocene, a thermal maximum occurred between 10 and 5.7 cal ka BP (440 cm), with the highest MAT values reaching ca. 10°C.

At ~6.5 cal ka BP, the MAT decreased for both calibrations. The temperature drop coincides with organic-poor layers in the sediment core formed during a drought, ~~concurring~~ associated with low monsoonal intensity (Bittner et al., 2020). ~~While drought phases are not directly linked to changing temperatures, in the monsoonal systems of eastern Africa, temperature and precipitation seem to be more connected (Costa et al., 2014; Loomis et al., 2015).~~

A strong offset between the calibrations appeared at 4.2 cal ka BP, at a moment when temperatures are expected to decrease in phase with insolation (Fig. 7). Using the MBT'$_{5ME}$, we reconstruct a sudden temperature rise (Fig. 7) that contrasts with the temperature decrease when using the MBT'$_{5ME}$ + IIIa' calibration ~~at a moment when temperatures are expected to decrease in phase with insolation (Fig. 7)~~. The offset coincides with a known drought phase and is

accompanied by shifts of many proxies (TOC, $\delta^{13}C$, TOC/N, *Erica spp*, charcoal) in the Garba Guracha sediments ~~record~~ (Bittner et al., 2020; Gil-Romera et al., 2019). The changing conditions in the Garba Guracha catchment during this drought phase, especially the decline of the *Erica* shrubland (Gil-Romera et al., 2019), might have ~~resulted in an increased~~ increased the ~~lake~~ surface water pH (Fig.5). A change in the lake water chemistry is supported ~~by a decrease in CBT' ratio and~~ changes in the reconstructed surface water pH (7.3-9.1) and conductivity (30 – 189; reported in Fig. 5 as ln(conductivity)) of the lake water (Fig. 5; calibrations from Russel et al., 2018 and Raberg et al., 2021). ~~In In the Garba Guracha CBT', pH and conductivity show similar changes, and it has been shown on a global scale, that CBT' correlates with pH and conductivity (Raberg et al., 2021).~~ In the last years, studies have suggested that the change in brGDGT composition captured by the CBT' may change due to shifting bacterial communities in soils and lakes (De Jonge et al., 2019; van Bree et al., 2020; Weber et al., 2018). Previously, pH, conductivity and salinity-dependent brGDGTs composition, sometimes driven by ~~and~~ community changes have been shown to affect MBT'_{5ME} values in soils and lake sediments (De Jonge et al., 2021; Wang et al., 2021; Raberg et al., 2021), and we propose that a similar effect can be seen in Garba Guracha.

Hence we suggest that MBT'_{5ME} systematically overestimates the temperatures of Garba Guracha during the late Holocene after 4 cal ka BP. A systematic offset is further supported by continuously and similarly decreasing reconstructed temperatures using both calibrations until the top of the core with a shared maximum at 150 cm (1.6 cal ka BP). We suggest that the production of IIIa' at the expense of IIIa is increased during dryer intervals, possibly caused by a change in lake water chemistry and/or bacterial communities. We conclude that a temperature calibration including IIIa' allows to reconstruct MAT in Garba Guracha sediments more accurately, as it accounts for the unique and variable production of IIIa' in Bale Mountain lakes.

5.3 Paleotemperature reconstructions for the Garba Guracha sedimentary record – regional comparison

In contrast to precipitation reconstructions based on δ^2H in East Africa (Garelick et al. 2021), the temperature records do not show a clear meridional, north-south temperature change, nor an east-west pattern. The reconstructed overall temperature ranges are, however, consistent with the elevations of the lake archives. The amplitude of temperature change over the last 13 ka at Garba Guracha is ~6°C. Similar amplitudes of change have been reconstructed at other high-altitude sites (Lake Mahoma and Lake Rutundu) (Loomis et al. 2017; Garelick et al. 2022), whereas equatorial records at lower elevations yield lower temperature amplitudes (Lake Victoria and Lake Tanganyika) (Tierney et al. 2008; Berke et al. 2012), and higher temperature amplitudes are also recorded in northeast African Lake Tana (Loomis

et al. 2015). In fact, Garba Guracha has some of the highest amplitude temperature changes of all of the sites during the Holocene, perhaps because it combines high elevation with a slightly higher latitude than other terrestrial African temperature records.

5.3.1. Deglacial warming

Overall, the recorded temperature trends in Garba Guracha are in phase with northern summer insolation variability (Fig. 8). This is reasonable because air temperature and insolation are closely connected (Huybers, 2006). However, the coldest MATs (<5°C) were recorded before 10.5 cal ka BP even though the northern hemisphere summer (20°N) insolation maxima occurred already 12 cal ka BP (Fig. 8). Tiercelin et al. (2008) argue that in Garba Guracha, ice remained in the catchment until ~10 cal ka BP due to topographical conditions, especially the north-facing exposition of the valley. The remaining ice in the basin might have (i) reduced the temperature of the lake water by inflow of cold melt water and (ii) buffered the air temperature warming caused by increasing insolation. Indeed, rising temperatures were recorded in other eastern African records as early as ~~14~~ 21 cal ka BP (Lake ~~Tana~~Mahoma) (Garelick et al., 2022) and in Ethiopia as early as 14 cal ka BP (Lake Tana) (Loomis et al., 2015; Tierney et al., 2016).

Similar to Lake Tana, but ~4000 years later, MAT (°C) in the Garba Guracha record experienced an abrupt increase of ca. 3.5°C in just ca. 600 years, from 10.5 to 9.9 cal ka BP. Simultaneously with the rise in temperature, Bittner et al. (2021) found an increase in P/E, indicating higher moisture availability based on depleting values of reconstructed $\delta^{18}O_{lake\ water}$. At Lake Tana, Loomis et al. (2015) and Costa et al. (2014) attribute a similar connection between warmer temperature and depleted water isotopes ($\delta^{2}H$) since 13.8 cal ka BP to the penetration of warm Congo Basin air masses resulting in weaker easterly trade winds and a strengthening of the southwesterly winds and the Somali Jet. The connection between Congo Basin air masses and eastern Africa is supported by the absence of cold temperatures associated with the Younger Dryas (YD) in both the Congo Basin temperature record (Weijers et al., 2007a) and Lake Tana (Loomis et al., 2015). However, in the Garba Guracha record, lower temperatures prevailed 4000 years longer than in Lake Tana (Loomis et al., 2015). Although catchment glaciers could have caused these conditions in Garba Guracha, the low temperatures are accompanied by a reduced sedimentation rate between 12.8 and 11.3 cal ka BP (Bittner et al., 2020), pointing to climatic influences associated with YD times (Alley, 2000). Indeed, other records from the Horn of Africa indicate dry conditions associated with the YD period, like Lake Ashenge (Marshall et al., 2009) and the marine record of the Gulf of Aden (Tierney and deMenocal, 2013). Therefore, we suggest that, at least for some periods, the

433 climate drivers operating in the Garba Guracha region might have been different from other parts of eastern Africa.
434 The time lag between Lake Tana and Garba Guracha could be explained by a slow eastwards advance of the Congo
435 Air Boundary and different climatic conditions at the sites. However, with the current data, we are unable to precisely
436 distinguish between north hemisphere YD forcing, remaining ice in the lake catchment, or regional atmospheric cir-
437 culation change affecting the Garba Guracha record.

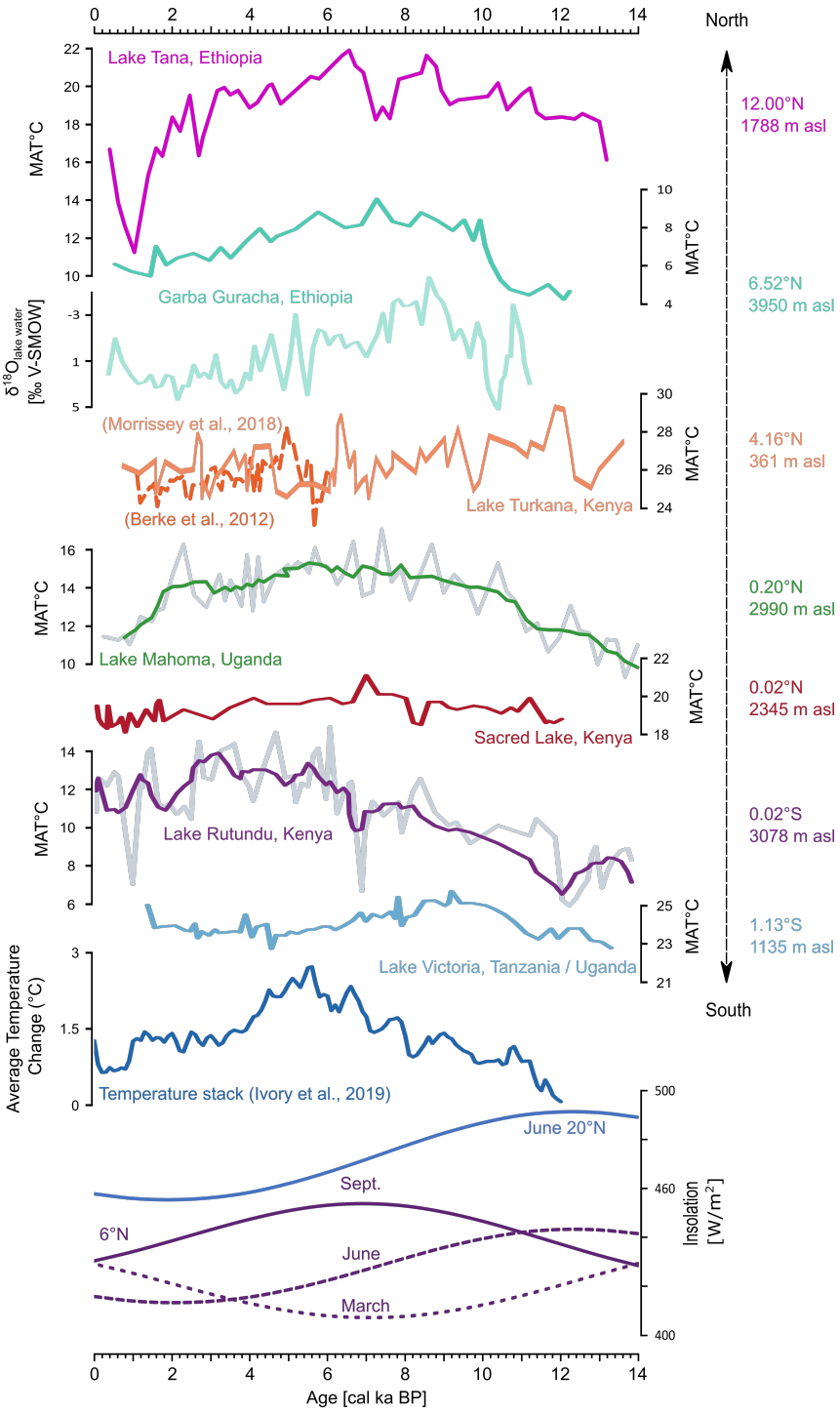

438

439 Figure 8: Comparison of records. MAT: Lake Tana (Loomis et al., 2015); Garba Guracha (this study); $\delta^{18}O_{lake\ water}$ as reconstructed from the aquatic
440 sugar biomarker fucose (Bittner et al., 2021); Lake Turkana (Berke et al., 2012; Morrissey et al., 2018); Lake Mahoma (Garelick et al., 2022); Sacred
441 Lake (Loomis et al., 2012); Lake Rutundu (Loomis et al., 2017); Lake Victoria (Berke et al., 2012); eastern Africa temperature stack (Ivory et al.,
442 2019); and insolation 6°N and June 20°N (Laskar et al., 2004).

443 5.3.2. Warm temperatures during the African Humid Period in eastern Africa

444 Regardless of the cause, the ~10.5 cal ka BP rise in MAT is associated with an abrupt increasing moisture availability
445 and changes of vegetation around Garba Guracha (Gil-Romera et al., 2021; Umer et al., 2007). Vegetation and fire
446 dynamics around Garba Guracha responded dynamically to the changing climatic conditions, evidencing the sensitivity
447 of the afromontane-afroalpine plant communities to increasing temperature. As MAT increased between 11 and 10 cal
448 ka BP, the ericaceous belt expanded (Gil-Romera et al., 2021). The rising temperature and increasing P/E (Bittner et
449 al., 2021) were accompanied by the expansion of the afroalpine vegetation cover (Gil-Romera et al., 2021; Miehe and
450 Miehe, 1994). An immediate consequence of the temperature rise and increasing moisture availability was biomass
451 accumulation, as evidenced by the change from organic matter-poor to organic matter-rich sedimentation (Bittner et
452 al., 2020) and the expansion of heathlands (Gil-Romera et al., 2019). Under an increasing MAT and extending biomass,
453 fire activity was very intense at this time (Gil-Romera et al., 2019).

454 The thermal maximum of the Garba Guracha record spanned from 9 to 5.8 cal ka BP, with the highest reconstructed
455 temperatures occurring at 7 cal ka BP. A similar mid-Holocene thermal optimum has been recorded at Sacred Lake (7
456 cal ka BP) and Lake Tana (7 cal ka BP) (Fig 8). However, the highest temperatures of Lake Victoria occurred at 9 cal
457 ka BP, and of Lake Rutundu, Lake Malawi and Lake Tanganyika at 5 cal ka BP (Berke et al., 2012b; Loomis et al.,
458 2017, 2015, 2012; Powers et al., 2005; Tierney et al., 2008; Garelick et al., 2022). At Lake Turkana, the thermal
459 optimum occurred at 6.4 cal ka BP (Morrissey et al., 2018) or 5 cal ka BP (Berke et al., 2012a). A new temperature
460 reconstruction from Lake Mahoma (Garelick et al., 2022) and a temperature stack including temperature reconstruc-
461 tions from Sacred Lake, Lake Malawi, Lake Tanganyika, Lake Rutundu, and the Congo Basin by Ivory and Russell
462 (2018) showed the highest temperatures between ~7 and ~4.5 cal ka BP. The timing of the highest reconstructed tem-
463 peratures at these sites is not related to greenhouse gas radiative forcing or insolation forcing (Loomis et al., 2015).
464 Loomis et al. (2015) point out that the Lake Tana and Sacred Lake temperature maxima lag northern hemisphere
465 summer insolation, and Lake Malawi and Lake Tanganyika lead peak southern summer insolation. In the case of Garba
466 Guracha, the highest temperatures coincide with local maximum September insolation at the sites latitude of 6°N
467 (Laskar et al., 2004) (Fig. 8). This matches the suggestion of Berke et al. (2012a) that the thermal optimum of several
468 eastern African lakes might be determined by local solar irradiance from Sep to Dec (maximum at ~6 cal ka BP) (Fig.
469 8) rather than northern hemisphere summer solar irradiance. The restratification processes of eastern African lakes in

these months and associated epilimnetic heating might explain the increased warming of lake water (Berke et al., 2012a). However, modelling studies do not support this hypothesis (Dee et al., 2021).

In addition to local insolation changes, local changes in P/E could have the potential to modify the lake water temperature. During the Early and Mid-Holocene, reconstructed high temperatures occurred during the African Humid Period, accompanied by the wettest phase of Garba Guracha (Bittner et al., 2021) and rising lake levels in the region (Gasse, 2000; Junginger et al., 2014), indicating higher amounts of precipitation due to an intensification of the monsoon system. A modelling study (Tierney et al., 2011b) proposes that during the AHP, the precipitation increase occurred mainly in June, July, and August (JJA), shortening the duration of annual drought phases in eastern Africa. Increased relative humidity would reduce evaporation, limiting the evaporative cooling of the lake water. Less evaporation, either due to shorter drought phases or generally higher precipitation, would increase the temperature and cause less positive $\delta^{18}O_{lake\ water}$ values, as suggested for Garba Guracha (Bittner et al., 2021).

The highest temperatures of the Holocene continued until 5.8 cal ka BP, interrupted only by a short drop in temperature after 7 cal ka BP. This is in agreement with the Sacred Lake temperature record (Loomis et al., 2012). Lake Tana experienced a shift towards colder conditions a bit earlier, from 7.5 to 7 cal ka BP (Loomis et al., 2015).

5.3.3. ~~cooling~~ Cooling in the Late Holocene

After 5.8 cal ka BP, the MAT continuously decreased by ~3.6°C until recent times, coinciding with the summer insolation decline and decreasing temperatures of equatorial lakes (Ivory and Russell, 2018), Lake Tana (Loomis et al., 2015) and the marine Gulf of Aden record (Tierney et al., 2016). The general decreasing temperature trend is also supported by $\delta^{18}O_{lake\ water}$, pollen and charcoal results showing a decrease in moisture availability and fire activity at Garba Guracha (Bittner et al., 2021; Gil-Romera et al., 2019). Furthermore, an upwards shift of the lower and dry forests during this time reinforces the idea of more intense evapotranspiration due to the decrease in moisture availability (Gil-Romera et al., 2021). A drop in TOC and decreasing $\delta^{13}C$ values (Bittner et al., 2020) support overall shifting catchment conditions.

During the last two thousand years, we observed that the increasing temperature trend concurred with an abrupt increase in the main woody communities and enhanced fire activities around Garba Guracha (Gil-Romera et al., 2021). However, we cannot discard human influence ~~favouring~~favoring both woody encroachment and fire activity.

The strong connection of temperature, P/E and insolation across the Holocene shows that the Garba Guracha temperatures might have been affected by local radiation, possibly in interplay with insolation-driven atmospheric circulation changes and their impacts on air mass source, cloud cover and evaporation. As current global warming continues, the intense warming of landmasses could lead to a major and complex restructuring of the atmospheric circulation system in the future, affecting eastern Africa and possibly even larger regions beyond via teleconnections.

6. CONCLUSIONS

Eastern African climatic history is spatially very diverse, and the driving mechanisms are complex and not fully understood. In eastern Africa, temperature reconstructions are generally sparse, especially in the high altitudes of the Horn of Africa. In this study, we used brGDGT from a high altitude sedimentary record of the Bale Mountains (lake Garba Guracha, Southwestern Ethiopia) to produce the first temperature reconstruction for the Horn of Africa.

The composition of brGDGT isomers in sediment records is affected by several influences, mainly by MAT, but in addition by lake water chemistry (~~like~~ pH and conductivity) and bacterial community, resulting in locally unique brGDGT compositions. For instance, in some of the Bale Mountain lakes, the abundance of a specific isomer IIIa' is uncommonly high in surface sediments. However, the summed abundance of IIIa and IIIa' is similar to other comparable lake archives in eastern Africa. We suspect that in the case of the Bale Mountains, changes in the lake's water chemistry (~~like~~ pH and conductivity) or bacterial community are responsible for the high production of IIIa' at the expense of IIIa under drier conditions. By including the 6 methyl isomer in a temperature calibration, we were able to enhance the correlation with MAT. Therefore, we conclude that 6 methyl isomers have an impact on temperature reconstructions, highlighting their inclusion in a Bale Mountain-specific temperature calibration. Using surface sediment data from Bale Mountain lakes and the East African lake database, the best performing temperature calibration is a modified MBT'_{5ME} including IIIa'.

With the use of the new calibration, the Garba Guracha MAT record reflects insolation variability as one of the main climatic drivers at millennial scales. Additional factors such as glacier and permafrost melting during deglaciation and the regional atmospheric circulation likely play a prominent role on shorter time scales. These additional mechanisms partly explain the asynchronicity between the Garba Guracha MAT record in the high altitude afro-alpine region of the Horn of Africa and other eastern African lake records.

Further research is necessary to understand the influences on and the origin of brGDGTs producing communities, especially at high altitudes.

Author contribution. LB, GGR, HFL, and MZ collected the samples. LB, CDJ, JMR and MZ developed the concept. LB and CDJ extracted, ~~analyzed~~ analysed and interpreted the brGDGT data. LB led the manuscript writing with contributions and feedback from all authors. MZ acquired the funding and supervised the work.

Competing interests. The authors declare that they have no conflict of interest.

Acknowledgements

This research was funded by the German Research Council (DFG: ZE 844/10–1) in the framework of the joint Ethio-European DFG Research Unit 2358 "The Mountain Exile Hypothesis. How humans benefited from and reshaped African high-altitude ecosystems during Quaternary climate changes". We are grateful to the project coordination, the Philipps University Marburg, the University of Addis Abeba, the Frankfurt Zoological Society, the Ethiopian Wolf Project, the Bale Mountains National Park, and the related staff members, especially Katinka Thielsen and Mekbib Fekadu for their logistic assistance during our fieldwork. We thank the Ethiopian Wildlife Conservation Authority for permitting our research in the Bale Mountains National Park.

7. REFERENCES

Alley, R. B.: The Younger Dryas cold interval as viewed from central Greenland, Quaternary Science Reviews, 19, 213–226, https://doi.org/https://doi.org/10.1016/S0277-3791(99)00062-1, 2000.

Baxter, A. J., Hopmans, E. C., Russell, J. M., and Sinninghe Damsté, J. S.: Bacterial GMGTs in East African lake sediments: Their potential as palaeotemperature indicators, Geochimica et Cosmochimica Acta, 259, 155–169, https://doi.org/10.1016/j.gca.2019.05.039, 2019.

Berke, M. A., Johnson, T. C., Werne, J. P., Schouten, S., and Sinninghe Damsté, J. S.: A mid-Holocene thermal maximum at the end of the African Humid Period, Earth and Planetary Science Letters, 351–352, 95–104, https://doi.org/10.1016/j.epsl.2012.07.008, 2012a.

Berke, M. A., Johnson, T. C., Werne, J. P., Grice, K., Schouten, S., and Sinninghe Damsté, J. S.: Molecular records of

549 climate variability and vegetation response since the Late Pleistocene in the Lake Victoria basin, East Africa,
550 Quaternary Science Reviews, 55, 59–74, https://doi.org/10.1016/j.quascirev.2012.08.014, 2012b.
551 Bini, M., Zanchetta, G., Perşoiu, A., Cartier, R., Català, A., Cacho, I., Dean, J. R., Di Rita, F., Drysdale, R. N., Finnè,
552 M., Isola, I., Jalali, B., Lirer, F., Magri, D., Masi, A., Marks, L., Mercuri, A. M., Peyron, O., Sadori, L., Sicre, M.-A.,
553 Welc, F., Zielhofer, C., and Brisset, E.: The 4.2 ka BP Event in the Mediterranean region: an overview, Clim. Past, 15,
554 555–577, https://doi.org/10.5194/cp-15-555-2019, 2019.
555 Bittner, L., Bliedtner, M., Grady, D., Gil-Romera, G., Martin-Jones, C., Lemma, B., Mekonnen, B., Lamb, H. F., Yang,
556 H., Glaser, B., Szidat, S., Salazar, G., Rose, N. L., Opgenoorth, L., Miehe, G., Zech, W., and Zech, M.: Revisiting
557 afro-alpine Lake Garba Guracha in the Bale Mountains of Ethiopia: rationale, chronology, geochemistry, and
558 paleoenvironmental implications, Journal of Paleolimnology, https://doi.org/10.1007/s10933-020-00138-w, 2020.
559 Bittner, L., Gil-Romera, G., Grady, D., Lamb, H. F., Lorenz, E., Weiner, M., Meyer, H., Bromm, T., Glaser, B., and
560 Zech, M.: The Holocene lake-evaporation history of the afro-alpine Lake Garba Guracha in the Bale Mountains,
561 Ethiopia, based on $\delta^{18}O$ records of sugar biomarker and diatoms, Quaternary Research, 1–14,
562 https://doi.org/10.1017/qua.2021.26, 2021.
563 Blom, R. G., Farr, T. G., Feynmann, J., Ruzmaikin, A., and Paillou, P.: The green Sahara: Climate change, hydrologic
564 history and human occupation, in: 2009 IEEE Radar Conference, 1–4, https://doi.org/10.1109/RADAR.2009.4977129,
565 2009.
566 Bonnefille, R., Chalié, F., Guiot, J., and Vincens, A.: Quantitative estimates of full glacial temperatures in equatorial
567 Africa from palynological data*, Climate Dynamics, 6, 251–257, https://doi.org/10.1007/BF00193538, 1992.
568 van Bree, L. G. J., Peterse, F., Baxter, A. J., De Crop, W., van Grinsven, S., Villanueva, L., Verschuren, D., and
569 Sinninghe Damsté, J. S.: Seasonal variability and sources of in situ brGDGT production in a permanently stratified
570 African crater lake, Biogeosciences Discuss., 2020, 1–36, https://doi.org/10.5194/bg-2020-233, 2020.
571 Castañeda, I. S., Schouten, S., Pätzold, J., Lucassen, F., Kasemann, S., Kuhlmann, H., and Schefuß, E.: Hydroclimate
572 variability in the Nile River Basin during the past 28,000 years, Earth and Planetary Science Letters, 438, 47–56,
573 https://doi.org/10.1016/j.epsl.2015.12.014, 2016.
574 Cheddadi, R., Lamb, H. F., Guiot, J., and van der Kaars, S.: Holocene climatic change in Morocco: a quantitative
575 reconstruction from pollen data, Climate Dynamics, 14, 883–890, https://doi.org/10.1007/s003820050262, 1998.
576 Chevalier, M. and Chase, B. M.: Southeast African records reveal a coherent shift from high- to low-latitude forcing
577 mechanisms along the east African margin across last glacial–interglacial transition, Quaternary Science Reviews, 125,

578 117–130, https://doi.org/10.1016/j.quascirev.2015.07.009, 2015.
579 Costa, K., Russell, J., Konecky, B., and Lamb, H.: Isotopic reconstruction of the African Humid Period and Congo Air
580 Boundary migration at Lake Tana, Ethiopia, Quaternary Science Reviews, 83, 58–67,
581 https://doi.org/10.1016/j.quascirev.2013.10.031, 2014.
582 Damsté, J. S. S., Hopmans, E. C., Pancost, R. D., Schouten, S., and Geenevasen, J. A. J.: Newly discovered non-
583 isoprenoid glycerol dialkyl glycerol tetraether lipids in sediments, Chemical Communications, 1683–1684,
584 https://doi.org/10.1039/b004517i, 2000.
585 Dearing Crampton-Flood, E., Tierney, J. E., Peterse, F., Kirkels, F. M. S. A., and Sinninghe Damsté, J. S.: BayMBT:
586 A Bayesian calibration model for branched glycerol dialkyl glycerol tetraethers in soils and peats, Geochimica et
587 Cosmochimica Acta, 268, 142–159, https://doi.org/https://doi.org/10.1016/j.gca.2019.09.043, 2020.
588 Dee, S. G., Morrill, C., Kim, S. H., and Russell, J. M.: Hot Air, Hot Lakes, or Both? Exploring Mid-Holocene African
589 Temperatures Using Proxy System Modeling, Journal of Geophysical Research: Atmospheres, 126, e2020JD033269,
590 https://doi.org/https://doi.org/10.1029/2020JD033269, 2021.
591 deMenocal, P., Ortiz, J., Guilderson, T., Adkins, J., Sarnthein, M., Baker, L., and Yarusinsky, M.: Abrupt onset and
592 termination of the African Humid Period:, Quaternary Science Reviews, 19, 347–361, https://doi.org/10.1016/S0277-
593 3791(99)00081-5, 2000.
594 Eggermont, Windafrash, M., Van Damme, M., Lens, K., and Umer M., H.: Bale Moluntains Lakes : Ecosystems under
595 pressure of global change?, Walia, 2011, 171–180, https://doi.org/10.10520/AJA00837059_148, 2011.
596 Eggermont, H., Heiri, O., James, A., Ae, R., Vuille, M., Leen, A., Ae, A., and Verschuren, D.: Paleotemperature
597 reconstruction in tropical Africa using fossil Chironomidae (Insecta: Diptera), Journal of Paleolimnology, 43, 413–
598 435, https://doi.org/10.1007/s10933-009-9339-2, 2010.
599 Garelick, S., Russell, J., Richards, A., Smith, J., Kelly, M., Anderson, N., Jackson, M. S., Doughty, A., Nakileza, B.,
600 Ivory, S., Dee, S., and Marshall, C.: The dynamics of warming during the last deglaciation in high-elevation regions
601 of Eastern Equatorial Africa, Quaternary Science Reviews, 281, 107416,
602 https://doi.org/10.1016/j.quascirev.2022.107416, 2022.
603 Gasse, F.: Hydrological changes in the African tropics since the Last Glacial Maximum, Quaternary Science Reviews,
604 19, 189–211, https://doi.org/https://doi.org/10.1016/S0277-3791(99)00061-X, 2000.
605 Gil-Romera, G., Adolf, C., Benito Blas, M., Bittner, L., Johansson, M. M. U., Grady, D. D. A., Lamb, H. H. F., Lemma,
606 B., Fekadu, M., Glaser, B., Mekonnen, B., Sevilla-Callejo, M., Zech, M., Zech, W., Miehe, G., Benito, B. M., Bittner,

L., Johansson, M. M. U., Grady, D. D. A., Lamb, H. H. F., Lemma, B., Fekadu, M., Glaser, B., Mekonnen, B., Sevilla-Callejo, M., Zech, M., Zech, W., and Miehe, G.: Long-term fire resilience of the Ericaceous Belt, Bale Mountains, Ethiopia, Biology Letters, 15, 20190357, https://doi.org/10.1098/rsbl.2019.0357, 2019.

Gil-Romera, G., Fekadu, M., Opgenoorth, L., Grady, D., Lamb, H. F., Bittner, L., Zech, M., and Miehe, G.: The new Garba Guracha palynological sequence: Revision and data expansion, in: Quaternary Vegetation Dynamics – The African Pollen Database, edited by: Runge, J., Gosling, W.D., Lézine, A-M., S. L., CRC Press, London, 442, https://doi.org/10.1201/9781003162766, 2021.

Groos, A., Akçar, N., Yesilyurt, S., Miehe, G., Vockenhuber, C., and Veit, H.: Nonuniform Late Pleistocene glacier fluctuations in tropical Eastern Africa, Science Advances, 7, https://doi.org/10.1126/sciadv.abb6826, 2021.

Groos, A. R., Niederhauser, J., Wraase, L., Hänsel, F., Nauss, T., Akçar, N., and Veit, H.: Implications of present ground temperatures and relict stone stripes in the Ethiopian Highlands for the palaeoclimate of the tropics, Earth Surf. Dynam. Discuss., 2020, 1–37, https://doi.org/10.5194/esurf-2020-53, 2020.

Hillman, J.: The Bale Mountains National Park Area, Southeast Ethiopia, and Its Management, 253 pp., https://doi.org/10.2307/3673456, 1988.

Hopmans, E. C., Weijers, J. W. H., Schefuß, E., Herfort, L., Sinninghe Damsté, J. S., and Schouten, S.: A novel proxy for terrestrial organic matter in sediments based on branched and isoprenoid tetraether lipids, Earth and Planetary Science Letters, 224, 107–116, https://doi.org/10.1016/j.epsl.2004.05.012, 2004.

Hopmans, E. C., Schouten, S., and Sinninghe Damsté, J. S.: The effect of improved chromatography on GDGT-based palaeoproxies, Organic Geochemistry, 93, 1–6, https://doi.org/https://doi.org/10.1016/j.orggeochem.2015.12.006, 2016.

Hove, H., Echeverria, D., and Parry, J.-E.: Review of current and planned adaptation action: East Africa, International Institute for Sustainable Development, Winnipeg, 2011.

Hughes, A. C., Orr, M. C., Ma, K., Costello, M. J., Waller, J., Provoost, P., Yang, Q., Zhu, C., and Qiao, H.: Sampling biases shape our view of the natural world, Ecography, 44, 1259–1269, https://doi.org/https://doi.org/10.1111/ecog.05926, 2021.

Huguet, C., Kim, J. H., Damsté, J. S. S., and Schouten, S.: Reconstruction of sea surface temperature variations in the Arabian Sea over the last 23 kyr using organic proxies (TEX86 and $U_{37}K'$), Paleoceanography, 21, https://doi.org/10.1029/2005PA001215, 2006.

Huybers, P.: Early Pleistocene Glacial Cycles and the Integrated Summer Insolation Forcing, Science (New York,

636 N.Y.), 313, 508–511, https://doi.org/10.1126/science.1125249, 2006.
637 IPCC: Climate Change 2021: The Physical Science Basis. Contribution of Working Group I to the Sixth Assessment
638 Report of the Intergovernmental Panel on Climate Change [Masson-Delmotte, V., P. Zhai, A. Pirani, S.L. Connors, C.
639 Péan, S. Berger, N. Caud, Y. Chen, Cambridge University Press, 2021.
640 Ivory, S. J. and Russell, J.: Lowland forest collapse and early human impacts at the end of the African Humid Period
641 at Lake Edward, equatorial East Africa, Quaternary Research, 89, 7–20, https://doi.org/10.1017/qua.2017.48, 2018.
642 Jaeschke, A., Thienemann, M., Schefuß, E., Urban, J., Schäbitz, F., Wagner, B., and Rethemeyer, J.: Holocene
643 Hydroclimate Variability and Vegetation Response in the Ethiopian Highlands (Lake Dendi), Frontiers in Earth
644 Science, 8, 1–14, https://doi.org/10.3389/feart.2020.585770, 2020.
645 De Jonge, C., Hopmans, E. C., Zell, C. I., Kim, J.-H., Schouten, S., and Sinninghe Damsté, J. S.: Occurrence and
646 abundance of 6-methyl branched glycerol dialkyl glycerol tetraethers in soils: Implications for palaeoclimate
647 reconstruction, Geochimica et Cosmochimica Acta, 141, 97–112, https://doi.org/10.1016/j.gca.2014.06.013, 2014.
648 De Jonge, C., Radujković, D., Sigurdsson, B. D., Weedon, J. T., Janssens, I., and Peterse, F.: Lipid biomarker
649 temperature proxy responds to abrupt shift in the bacterial community composition in geothermally heated soils,
650 Organic Geochemistry, 137, https://doi.org/10.1016/j.orggeochem.2019.07.006, 2019.
651 De Jonge, C., Kuramae, E. E., Radujković, D., Weedon, J. T., Janssens, I. A., and Peterse, F.: The influence of soil
652 chemistry on branched tetraether lipids in mid- and high latitude soils: Implications for brGDGT- based
653 paleothermometry, Geochimica et Cosmochimica Acta, 310, 95–112,
654 https://doi.org/https://doi.org/10.1016/j.gca.2021.06.037, 2021.
655 Junginger, A., Roller, S., Olaka, L. A., and Trauth, M. H.: The effects of solar irradiation changes on the migration of
656 the Congo Air Boundary and water levels of paleo-Lake Suguta , Northern Kenya Rift , during the African Humid
657 Period (15 – 5 ka BP), Palaeogeography, Palaeoclimatology, Palaeoecology, 396, 1–16,
658 https://doi.org/10.1016/j.palaeo.2013.12.007, 2014.
659 Kassambara, A. and Mundt, F.: factoextra: Extract and Visualize the Results of Multivariate Data Analyses,
660 https://cran.r-project.org/package=factoextra, 2020.
661 Kidane, Y., Stahlmann, R., and Beierkuhnlein, C.: Vegetation dynamics, and land use and land cover change in the
662 Bale Mountains, Ethiopia, Environmental Monitoring and Assessment, 184, 7473–7489,
663 https://doi.org/10.1007/s10661-011-2514-8, 2012.
664 Laskar, J., Robutel, P., Joutel, F., Gastineau, M., Correia, A. C. M., and Levrard, B.: A long-term numerical solution

665 for the insolation quantities of the Earth , A&A, 428, 261–285, 2004.
666 Löffler, H.: Limnology and paleolimnological data on the Bale Mountain Lakes, Verth, International Verein.
667 Limnology, 20, 1131–1138, 1978.
668 Loomis, S. E., Russell, J. M., and Sinninghe Damsté, J. S.: Distributions of branched GDGTs in soils and lake
669 sediments from western Uganda: Implications for a lacustrine paleothermometer, Organic Geochemistry, 42, 739–751,
670 https://doi.org/10.1016/j.orggeochem.2011.06.004, 2011.
671 Loomis, S. E., Russell, J. M., Heureux, A. M., D'Andrea, W. J., and Sinninghe Damsté, J. S.: Seasonal variability of
672 branched glycerol dialkyl glycerol tetraethers (brGDGTs) in a temperate lake system, Geochimica et Cosmochimica
673 Acta, 144, 173–187, https://doi.org/10.1016/j.gca.2014.08.027, 2014.
674 Loomis, S. E., Russell, J. M., and Lamb, H. F.: Northeast African temperature variability since the Late Pleistocene,
675 Palaeogeography, Palaeoclimatology, Palaeoecology, 423, 80–90, https://doi.org/10.1016/j.palaeo.2015.02.005, 2015.
676 Loomis, S. E., Russell, J. M., Verschuren, D., Morrill, C., De Cort, G., Sinninghe Damsté, J. S., Olago, D., Eggermont,
677 H., Street-Perrott, F. A., and Kelly, M. A.: The tropical lapse rate steepened during the Last Glacial Maximum, Science
678 Advances, 3, https://doi.org/10.1126/sciadv.1600815, 2017.
679 Loomis, S. E. S. E., Russell, J. M., Ladd, B., Street-Perrott, F. A. A., and Sinninghe Damsté, J. S. J. S.: Calibration
680 and application of the branched GDGT temperature proxy on East African lake sediments, Earth and Planetary Science
681 Letters, 357–358, 277–288, https://doi.org/https://doi.org/10.1016/j.epsl.2012.09.031, 2012.
682 Lyon, B. and Vigaud, N.: Unraveling East Africa's Climate Paradox,
683 https://doi.org/https://doi.org/10.1002/9781119068020.ch16, 22 June 2017.
684 Marshall, M., Lamb, H., Davies, S., Leng, M., Bedaso, Z., Umer, M., and Bryant, C.: Climatic change in northern
685 Ethiopia during the past 17,000 years: A diatom and stable isotope record from Lake Ashenge, Palaeogeography
686 Palaeoclimatology Palaeoecology, 279, https://doi.org/10.1016/j.palaeo.2009.05.003, 2009.
687 Martínez-Sosa, P., Tierney, J. E., Stefanescu, I. C., Crampton-Flood, E. D., Shuman, B. N., and Routson, C.: A global
688 Bayesian temperature calibration for lacustrine brGDGTs, https://doi.org/10.1594/PANGAEA.931169, 6 May 2021.
689 Miehe, S. and Miehe, G.: Ericaceous forests and heathlands in the Bale mountains of South Ethiopia : ecology and
690 man's impact, edited by: Miehe, G. and 1952-, Reinbek : Warnke, Reinbek, 1994.
691 Morrissey, A. and Scholz, C. A. C. A. C. A.: Paleohydrology of Lake Turkana and its influence on the Nile River
692 system, Palaeogeography, Palaeoclimatology, Palaeoecology, 403, 88–100,
693 https://doi.org/https://doi.org/10.1016/j.palaeo.2014.03.029, 2014.

Morrissey, A., Scholz, C. A., and Russell, J. M.: Late Quaternary TEX_{86} paleotemperatures from the world's largest desert lake, Lake Turkana, Kenya, Journal of Paleolimnology, 59, 103–117, https://doi.org/10.1007/s10933-016-9939-6, 2018.

Neukom, R., Barboza, L. A., Erb, M. P., Shi, F., Emile-Geay, J., Evans, M. N., Franke, J., Kaufman, D. S., Lücke, L., Rehfeld, K., Schurer, A., Zhu, F., Brönnimann, S., Hakim, G. J., Henley, B. J., Ljungqvist, F. C., McKay, N., Valler, V., von Gunten, L., and Consortium, P. 2k: Consistent multidecadal variability in global temperature reconstructions and simulations over the Common Era, Nature Geoscience, 12, 643–649, https://doi.org/10.1038/s41561-019-0400-0, 2019.

Nicholson, S. E.: Climate and climatic variability of rainfall over eastern Africa, Reviews of Geophysics, 55, 590–635, https://doi.org/https://doi.org/10.1002/2016RG000544, 2017.

Osmaston, H. A., Mitchell, W. A., and Osmaston, J. A. N.: Quaternary glaciation of the Bale Mountains, Ethiopia, Journal of Quaternary Science, 20, 593–606, https://doi.org/10.1002/jqs.931, 2005.

Ossendorf, G., Groos, A., Bromm, T., Girma Tekelemariam, M., Glaser, B., Lesur, J., Schmidt, J., Akçar, N., Bekele, T., Beldados, A., Demissew, S., Hadush Kahsay, T., P Nash, B., Nauss, T., Negash, A., Nemomissa, S., Veit, H., Vogelsang, R., Zerihun, W., and Miehe, G.: Middle Stone Age foragers resided in high elevations of the glaciated Bale Mountains, Ethiopia, Science, 365, 583–587, 2019.

Otto-Bliesner, B. L., Russell, J. M., Clark, P. U., Liu, Z., Overpeck, J. T., Konecky, B., DeMenocal, P., Nicholson, S. E., He, F., and Lu, Z.: Coherent changes of southeastern equatorial and northern African rainfall during the last deglaciation, Science, 346, 1223–1227, https://doi.org/10.1126/science.1259531, 2014.

Peterse, F., van der Meer, J., Schouten, S., Weijers, J. W. H., Fierer, N., Jackson, R. B., Kim, J.-H., and Sinninghe Damsté, J. S.: Revised calibration of the MBT–CBT paleotemperature proxy based on branched tetraether membrane lipids in surface soils, Geochimica et Cosmochimica Acta, 96, 215–229, https://doi.org/https://doi.org/10.1016/j.gca.2012.08.011, 2012.

Powers, L. A., Johnson, T. C., Werne, J. P., Castañeda, I. S., Hopmans, E. C., Sinninghe Damsté, J. S., and Schouten, S.: Large temperature variability in the southern African tropics since the Last Glacial Maximum, Geophysical Research Letters, 32, 1–4, https://doi.org/10.1029/2004GL022014, 2005.

R Core Team: R: A Language and Environment for Statistical Computing, https://www.r-project.org/, 2021.

Raberg, J. H., Harning, D. J., Crump, S. E., de Wet, G., Blumm, A., Kopf, S., Geirsdóttir, Á., Miller, G. H., and Sepúlveda, J.: Revised fractional abundances and warm-season temperatures substantially improve brGDGT

723 calibrations in lake sediments, Biogeosciences, 18, 3579–3603, https://doi.org/10.5194/bg-18-3579-2021, 2021.
724 Russell, J. M., Hopmans, E. C., Loomis, S. E., Liang, J., and Sinninghe Damsté, J. S.: Distributions of 5- and 6-methyl
725 branched glycerol dialkyl glycerol tetraethers (brGDGTs) in East African lake sediment: Effects of temperature, pH,
726 and new lacustrine paleotemperature calibrations, Organic Geochemistry, 117, 56–69,
727 https://doi.org/10.1016/j.orggeochem.2017.12.003, 2018.
728 Schouten, S., Forster, A., Panoto, F. E., and Sinninghe Damsté, J. S.: Towards calibration of the TEX_{86}
729 palaeothermometer for tropical sea surface temperatures in ancient greenhouse worlds, Organic Geochemistry, 38,
730 1537–1546, https://doi.org/10.1016/j.orggeochem.2007.05.014, 2007.
731 Schreuder, L. T., Beets, C. J., Prins, M. A., Hatté, C., and Peterse, F.: Late Pleistocene climate evolution in Southeastern
732 Europe recorded by soil bacterial membrane lipids in Serbian loess, Palaeogeography, Palaeoclimatology,
733 Palaeoecology, 449, 141–148, https://doi.org/https://doi.org/10.1016/j.palaeo.2016.02.013, 2016.
734 Sinninghe Damsté, J. S., Rijpstra, W. I. C., Foesel, B. U., Huber, K. J., Overmann, J., Nakagawa, S., Kim, J. J.,
735 Dunfield, P. F., Dedysh, S. N., and Villanueva, L.: An overview of the occurrence of ether- and ester-linked iso-
736 diabolic acid membrane lipids in microbial cultures of the Acidobacteria: Implications for brGDGT paleoproxies for
737 temperature and pH, Organic Geochemistry, 124, 63–76, https://doi.org/10.1016/j.orggeochem.2018.07.006, 2018.
738 Tiercelin, J. J., Gibert, E., Umer, M., Bonnefille, R., Disnar, J. R., Lézine, A. M., Hureau-Mazaudier, D., Travi, Y.,
739 Keravis, D., and Lamb, H. F.: High-resolution sedimentary record of the last deglaciation from a high-altitude lake in
740 Ethiopia, Quaternary Science Reviews, 27, 449–467, https://doi.org/10.1016/j.quascirev.2007.11.002, 2008.
741 Tierney, J. E. and deMenocal, P. B.: Abrupt Shifts in Horn of Africa Hydroclimate Since the Last Glacial Maximum,
742 Science, 342, 843–846, https://doi.org/10.1126/science.1240411, 2013.
743 Tierney, J. E. and Russell, J. M.: Abrupt climate change in southeast tropical Africa influenced by Indian monsoon
744 variability and ITCZ migration, Geophysical Research Letters, 34, https://doi.org/10.1029/2007GL029508, 2007.
745 Tierney, J. E., Russell, J. M., Huang, Y., Damste, J. S. S., Hopmans, E. C., and Cohen, A. S.: Northern Hemisphere
746 Controls on Tropical Southeast African Climate During the Past 60,000 Years, Science, 322, 252–255,
747 https://doi.org/10.1126/science.1160485, 2008.
748 Tierney, J. E., Russell, J. M., Sinninghe Damsté, J. S., Huang, Y., and Verschuren, D.: Late Quaternary behavior of
749 the East African monsoon and the importance of the Congo Air Boundary, Quaternary Science Reviews, 30, 798–807,
750 https://doi.org/10.1016/j.quascirev.2011.01.017, 2011a.
751 Tierney, J. E., Lewis, S. C., Cook, B. I., LeGrande, A. N., and Schmidt, G. A.: Model, proxy and isotopic perspectives

752 on the East African Humid Period, Earth and Planetary Science Letters, 307, 103–112,
753 https://doi.org/10.1016/j.epsl.2011.04.038, 2011b.
754 Tierney, J. E., Smerdon, J. E., Anchukaitis, K. J., and Seager, R.: Multidecadal variability in East African hydroclimate
755 controlled by the Indian Ocean, Nature, 493, 389–392, https://doi.org/10.1038/nature11785, 2013.
756 Tierney, J. E., Pausata, F. S. R., and Demenocal, P.: Deglacial Indian monsoon failure and North Atlantic stadials
757 linked by Indian Ocean surface cooling, Nature Geoscience, 9, 46–50, https://doi.org/10.1038/ngeo2603, 2016.
758 Tierney, J. E., Pausata, F. S. R., and DeMenocal, P. B.: Rainfall regimes of the Green Sahara, Science Advances, 3,
759 https://doi.org/10.1126/sciadv.1601503, 2017.
760 Trauth, M. H., Foerster, V., Junginger, A., Asrat, A., Lamb, H. F., and Schaebitz, F.: Abrupt or gradual? Change point
761 analysis of the late Pleistocene–Holocene climate record from Chew Bahir, southern Ethiopia, Quaternary Research,
762 90, 321–330, https://doi.org/DOI: 10.1017/qua.2018.30, 2018.
763 Uhlig, S. and Uhlig, K.: Studies on the Altitudinal Zonation of Forests and Alpine Plants in the Central Bale Mountains,
764 Ethiopia, 153 pp., https://doi.org/10.2307/3673574, 1991.
765 Uhlig, S. K.: Mountain Forests and the Upper Tree Limit on the Southeastern Plateau of Ethiopia, Mountain Research
766 and Development, 8, 227–234, https://doi.org/10.2307/3673452, 1988.
767 Umer, M., Lamb, H. F., Bonnefille, R., Lézine, A. M., Tiercelin, J. J., Gibert, E., Cazet, J. P., and Watrin, J.: Late
768 Pleistocene and Holocene vegetation history of the Bale Mountains, Ethiopia, Quaternary Science Reviews, 26, 2229–
769 2246, https://doi.org/10.1016/j.quascirev.2007.05.004, 2007.
770 Wagner, B., Wennrich, V., Viehberg, F., Junginger, A., Kolvenbach, A., Rethemeyer, J., Schaebitz, F., and Schmiedl,
771 G.: Holocene rainfall runoff in the central Ethiopian highlands and evolution of the River Nile drainage system as
772 revealed from a sediment record from Lake Dendi, Global and Planetary Change, 163, 29–43,
773 https://doi.org/10.1016/j.gloplacha.2018.02.003, 2018.
774 Wang, H., Liu, W., He, Y., Zhou, A., Zhao, H., Liu, H., Cao, Y., Hu, J., Meng, B., Jiang, J., Kolpakova, M.,
775 Krivonogov, S., and Liu, Z.: Salinity-controlled isomerization of lacustrine brGDGTs impacts the associated
776 MBT5ME' terrestrial temperature index, Geochimica et Cosmochimica Acta, 305, 33–48,
777 https://doi.org/https://doi.org/10.1016/j.gca.2021.05.004, 2021.
778 Weber, Y., Damsté, J. S. S., Zopfi, J., De Jonge, C., Gilli, A., Schubert, C. J., Lepori, F., Lehmann, M. F., and Niemann,
779 H.: Redox-dependent niche differentiation provides evidence for multiple bacterial sources of glycerol tetraether lipids
780 in lakes, Proceedings of the National Academy of Sciences of the United States of America, 115, 10926–10931,

https://doi.org/10.1073/pnas.1805186115, 2018.

Weijers, J. W. H., Schefuß, E., Schouten, S., and Damsté, J. S. S.: Coupled thermal and hydrological evolution of tropical Africa over the last deglaciation, Science, 315, 1701–1704, https://doi.org/10.1126/science.1138131, 2007a.

Weijers, J. W. H., Schouten, S., van den Donker, J. C., Hopmans, E. C., and Sinninghe Damsté, J. S.: Environmental controls on bacterial tetraether membrane lipid distribution in soils, Geochimica et Cosmochimica Acta, 71, 703–713, https://doi.org/10.1016/j.gca.2006.10.003, 2007b.

Werdecker, J.: Eine Durchquerung des Goba-Massivs in Südäthiopien, Hermann vo, 132–144, 1962.

Williams, F. M.: The Southeastern Highlands and the Ogaden, edited by: Williams, F. M., Springer International Publishing, Cham, 153–170, https://doi.org/10.1007/978-3-319-02180-5_15, 2016.

Woldu, Z., Feoli, E., and Nigatu, L.: Partitioning an elevation gradient of vegetation from southeastern Ethiopia by probabilistic methods, Plant Ecology, 81, 189–198, 1989.

Wu, H., Guiot, J., Brewer, S., and Guo, Z.: Climatic changes in Eurasia and Africa at the last glacial maximum and mid-Holocene: reconstruction from pollen data using inverse vegetation modelling, Climate Dynamics, 29, 211–229, https://doi.org/10.1007/s00382-007-0231-3, 2007.

Zeng, F. and Yang, H.: Temperature changes reconstructed from branched GDGTs on the central Loess Plateau during the past 130–5 ka, Quaternary International, 503, 3–9, https://doi.org/https://doi.org/10.1016/j.quaint.2018.04.045, 2019.